JGR Atmospheres

RESEARCH ARTICLE
10.1029/2024JD041407

Modeling the Effects of Vegetation and Snow on Dust Storm Over the Gobi Desert

Yueting Hao[1], Zilin Wang[1,2], Lian Xue[1,2], Sijia Lou[1], Ke Ding[1], Yue Qin[3], and Xin Huang[1,2]

[1]School of Atmospheric Sciences, Nanjing University, Nanjing, China, [2]Frontiers Science Center for Critical Earth Material Cycling, Nanjing University, Nanjing, China, [3]College of Environmental Sciences and Engineering, Peking University, Beijing, China

Key Points:

- Ground-based observations and satellite products are combined to indicate the correlation between dust storms and vegetation and snow cover
- A high-resolution dynamic dust source function, incorporating vegetation and snow factors, is developed for the GOCART-WRF dust scheme
- The dynamic dust source function improves model performance and demonstrates the vegetation and snow effects on dust over the Gobi region

Supporting Information:

Supporting Information may be found in the online version of this article.

Correspondence to:

X. Huang and Y. Qin,
xinhuang@nju.edu.cn;
qinyue@pku.edu.cn

Citation:

Hao, Y., Wang, Z., Xue, L., Lou, S., Ding, K., Qin, Y., & Huang, X. (2024). Modeling the effects of vegetation and snow on dust storm over the Gobi Desert. *Journal of Geophysical Research: Atmospheres*, *129*, e2024JD041407. https://doi.org/10.1029/2024JD041407

Received 22 APR 2024
Accepted 5 NOV 2024

Author Contributions:

Conceptualization: Yueting Hao, Xin Huang
Data curation: Yueting Hao
Formal analysis: Yueting Hao
Funding acquisition: Xin Huang
Investigation: Yueting Hao
Methodology: Yueting Hao, Lian Xue, Sijia Lou, Ke Ding, Xin Huang
Project administration: Xin Huang
Resources: Yueting Hao, Xin Huang
Software: Yueting Hao
Supervision: Yue Qin, Xin Huang
Validation: Yueting Hao
Visualization: Yueting Hao
Writing – original draft: Yueting Hao
Writing – review & editing: Yueting Hao, Lian Xue, Sijia Lou, Ke Ding, Yue Qin, Xin Huang

Abstract The Gobi Desert is a prominent dust source in Asia, where the dust storm is severe and features great interannual and seasonal variability. Previous studies have found land surface variation plausibly plays an important role in the occurrence and intensity of dust storms. However, the quantitative estimation and numerical description in current models are still limited. Here, a comprehensive study utilizing multiple observations and modeling methods to assess the influence of vegetation and snow on dust was conducted. We found that Gobi deserts exhibit substantial monthly and interannual variability in dust storms, which shows a close connection with vegetation and snow. To quantitatively understand the impact of vegetation and snow cover on dust emissions and also to better characterize such effects in numerical models, we introduced a high-resolution dynamic dust source function that incorporates the effects of vegetation and snow on erodibility. The new parameterization noticeably improved dust-related simulations, including aerosol optical thickness and PM_{10} concentrations, and provided insights into the distinct effects of vegetation and snow on dust emissions. This study sheds light on the effects of vegetation and snow on dust storms over the Gobi Desert, highlighting the importance of dynamic representation of time-varying surface properties in dust simulation.

Plain Language Summary In Asia, the Gobi Desert is an important source of dust storms, and severe ones frequently engulf densely populated eastern China. The dust storms feature great seasonal and spatial variations. By combining multiple observations and numerical simulations, we found that vegetation, snow and dust storms in the Gobi Desert show synchronous monthly and interannual variations. Sparse vegetation and rapid snowmelt could greatly facilitate dust occurrence and intensity. To quantitatively understand the impacts of changing vegetation and snow cover on dust emissions, we develop a new parametrization to characterize dynamic dust sources. This new modeling method is capable of better representing Gobi dust storms and demonstrating how plants and snow affect dust storms.

1. Introduction

Mineral dust is a significant contributor to atmospheric aerosol, with about 2 billion tons emitted into the atmosphere each year from deserts worldwide (Shepherd et al., 2016). Dust aerosols have a great impact on the Earth's radiative energy balance, global material cycles, human health, and socioeconomics (Falkowski et al., 1998; Middleton, 2017; Tegen et al., 1996; Tobias et al., 2019). As absorbing aerosols, dust aerosols are estimated to have a global radiative forcing of roughly -0.2 ± 0.5 W/m^2, potentially influencing climate and local meteorological conditions (Kok et al., 2023; L. Liu et al., 2016). Moreover, terrestrial elements can enter oceans via dust aerosols, providing nutrients for phytoplankton and contributing to the biogeochemical cycle (Hamilton et al., 2022; Tan & Wang, 2014). Dust aerosols can also affect air quality by directly promoting heterogeneous reactions on the particle surface and indirectly enhancing the stability of the boundary layer and exacerbating the ozone and secondary pollutant production (Tang et al., 2017; Z. Wang et al., 2020; Y. Yang et al., 2022). With substantial impacts on cities near dust source areas, dust aerosols can also lead to increased respiratory hospitalizations (ESCAP, 2021; Y. Tao et al., 2012).

Dust storms are affected by both climate conditions and human activities, mainly through the variations of dust emissions under meteorological conditions and surface features, while surface vegetation and snow cover are critical factors affecting surface properties. Vegetation plays a vital role in curtailing wind erosion, on the one hand, by increasing surface roughness and thus reducing surface wind speeds; on the other hand, by making the soil particles near the roots of the vegetation more tightly bound and less likely to detach from the surface

(Abdourhamane Touré et al., 2019; Jiang et al., 2019; Shao, 2008; Zender et al., 2003). Aside from vegetation, snow cover also acts as a suppressor of dust storms (L. Han et al., 2011; Kurosaki & Mikami, 2004; L. Wang et al., 2014). Snow inhibits dust emissions directly when it covers dust sources, and melting snow increases soil moisture, which also prevents dust outbreaks (Tanaka et al., 2011).

The chemical transport model has been serving as an indispensable way to understand dust and its environmental and climate interactions quantitatively (Ginoux et al., 2001; Grini et al., 2005; N. Mahowald et al., 2003; N. M. Mahowald et al., 2010; Mokhtari et al., 2012). Many schemes parameterize dust emission through different computational approaches taking into account the effects of dynamic variables such as vegetation and snow cover on dust emissions (Albani et al., 2014; Cakmur et al., 2006; Chappell et al., 2023; Okin, 2005, 2008; Sagar Prasad Parajuli & Zender, 2017; Tegen et al., 2002; Tegen & Miller, 1998; Zender et al., 2003, 2003, 2003). For example, the percentage of grid cells with a normalized vegetation index (NDVI) below a specific threshold was utilized as a bareness indicator (Y. Chen et al., 2023; Kim, Chin, Kemp, et al., 2017; Kim et al., 2013; Solomos et al., 2019). The Mineral Dust Entrainment and Deposition (DEAD) model assumes that vegetation and snow cover can constrain dust emissions in a linear relationship (Zender et al., 2003). Parajuli et al. (2017) developed a global dust source map related to landforms, the upstream drainage area and the visible reflectance. Kurosaki and Mikami (2004) proposed a parameterization scheme for the effect of snow cover on threshold wind speeds for dust outbreaks, demonstrating that snow cover can linearly increase threshold wind speeds. However, it is noted that many global dust emission studies still rely on static inputs, such as fixed vegetation cover and bare soil fraction, in global dust emission modeling (Albani et al., 2014; Chappell et al., 2023). Ginoux et al. (2004, 2001) introduced the Goddard Chemistry Aerosol Radiation and Transport (GOCART) model to simulate the emission and distribution of dust aerosols. The GOCART dust emission scheme has been embedded in the Weather Research and Forecasting model with chemistry (WRF-Chem) and has been widely applied and improved in numerous studies (Bran et al., 2022; Chow et al., 2014; Sagar P. Parajuli et al., 2022; Ukhov et al., 2021; Z. Wang et al., 2020; Zeng et al., 2019). A notable limitation of the GOCART-WRF dust emission scheme is its static dust source function, which does not account for seasonal and interannual variations in dust sources (Kim, Chin, Kemp, et al., 2017; Kim et al., 2013; LeGrand et al., 2019; H. Li et al., 2023). Consequently, the accuracy of dust emission simulations, which are proportional to the dust source function, may be compromised (Kim et al., 2013; Sekiyama et al., 2011).

Asia is the second largest dust source globally (Kok et al., 2023) and the Gobi Desert is the most important one witnessing intensive dust storms (Prospero et al., 2002). There is a clear seasonal variation in dust storms in the Gobi region (Shao et al., 2013). During the spring season, dust from the Gobi Desert triggered by Mongolian cyclones and cold fronts impacts not only China's interior but also neighboring countries and regions (Kimura, 2018; E.-H. Lee & Sohn, 2011; L. Yang et al., 2021; Zhou et al., 2018). Research has revealed that dust storms in the Gobi Desert are sensitive to factors such as changes in vegetation cover, abnormal rainfall (including snowfall) patterns, soil wetness, climate change, and overgrazing (J. Han et al., 2021; E.-H. Lee & Sohn, 2011; J. Li et al., 2022; Shao et al., 2013; Yin et al., 2022, 2023; Zender & Kwon, 2005). Numerous studies have explored the spatiotemporal variations of dust activities in the Gobi Desert in recent decades and discussed the relationship between vegetation, snow, and dust storms. Increases in soil moisture and vegetation cover can contribute to the decrease in dust emissions in East Asia during 2010–2017 compared to 2001 (C. Wu et al., 2022). The year 2023 witnessed the highest incidence of dusty weather events in China over the past decade (S. Chen et al., 2023). Yin et al. (2022, 2023) concluded that low precipitation, early snowmelt, and sparse vegetation in the Gobi Desert contribute to favorable dust source conditions for severe dust storms. However, the relationship between dust storms and the role of vegetation and snow in dust emissions is not yet fully understood (Kim, Chin, Remer, et al., 2017). Also, a comprehensive understanding of their impacts on dust emissions remains lacking.

This study aims to gain deeper insights into the correlation between vegetation, snow cover, and dust storms. We analyze their seasonal and interannual spatiotemporal variations using ground-based observations and satellite products. Additionally, we incorporate high-resolution terrain height data as well as monthly vegetation and snow cover data sets to develop a new dynamic dust source function for the GOCART-WRF dust emission scheme. Dust simulations focusing on the Gobi Desert from February to May 2023 are conducted using the WRF-Chem model version 4.4.1. Evaluation results prove that the dynamic dust source function markedly improves model performance. Furthermore, through sensitivity experiments, we assess the impact of vegetation and snow indexes on dust emissions separately. This paper is organized as follows: Section 2 outlines the data sources and the methodology used to develop the dynamic dust source function. Section 3.1 provides an in-depth analysis of the

spatial and temporal variability of vegetation, snow cover and dust storms from February to May 2010–2023. Section 3.2 compares the differences between the original dust source function and the new dynamic dust source function, analyzing the monthly variability of dust sources in 2023. Additionally, it analyzes the spatiotemporal impacts of each contributing factor on dust emissions. Section 3.3 evaluates the simulation results for static and dynamic dust sources. Section 4 summarizes our discussions and conclusions.

2. Methods and Data

2.1. Numerical Description of Dynamic Dust Sources

2.1.1. GOCART-WRF Dust Emission Scheme

The GOCART dust emission scheme, originally developed by Ginoux et al. (2001), has been integrated into WRF-Chem. In this study, this scheme is utilized to simulate dust emissions over the dust-source regions mainly in the Gobi Desert. The GOCART-WRF scheme estimates dust emissions using input parameters provided by the WRF-Chem model, including wind speed, soil moisture, air density, and erodibility. To be specific, the dust emission flux E_p for a size group p could be calculated by the expression:

$$E_p = \begin{cases} \mathrm{EROD} \cdot Cs_p U_{10\mathrm{m}}{}^2 (U_{10\mathrm{m}} - U_t), \text{ if } U_{10\mathrm{m}} > U_t \\ 0, \text{ if } U_{10\mathrm{m}} \le U_t \end{cases} \quad (1)$$

where C is a dimensional factor (1 μg s^2/m^5), s_p is the fraction of size group p within the soil, and $U_{10\mathrm{m}}$ is the horizontal wind speed at 10 m (m/s). U_t is the threshold velocity required for initiating wind erosion (m/s) and is a function of particle size, air density, and the time-varying land surface soil moisture θ_s. Dust emission ceases if θ_s falls below 0.5. EROD describes the fraction of an erodible grid cell and represents the probability of having accumulated sediments in a grid cell. Ginoux et al. (2001) suggested that erodibility is related to topography, and cumulative sediment locations can be identified by comparing the elevation of each grid point to the elevation of the surrounding hydrologic basin. The base dust source function EROD for the GOCART-WRF scheme is calculated as follows:

$$\mathrm{EROD} = \left(\frac{z_{\max} - z}{z_{\max} - z_{\min}} \right)^5 \quad (2)$$

where z represents the altitude at the grid, and $z_{\max}$ and $z_{\min}$ are the maximum and minimum elevations in the surrounding 10° × 10° topography, respectively. Elevation differences are raised to the fifth power to enhance topographic contrast. Additionally, EROD is a three-layer variable comprising 50% sand, 25% silt, and 25% clay.

2.1.2. Inclusion of Vegetation and Snow in Dynamic Dust Sources Representation

In the GOCART-WRF scheme, the bare soil surface is identified by removing vegetation and snow masks from the EROD map (Ginoux et al., 2001; LeGrand et al., 2019; Zhang et al., 2024), and dynamic variables such as soil moisture and surface wind speed are considered in calculating dust emissions. However, the dust source function EROD remains static. The effects of vegetation and snow on dust sources are inadequately represented. The Mineral Dust Entrainment and Deposition (DEAD) model assumes that vegetation constrains dust by linearly reducing the fraction of bare soil (Zender et al., 2003). To expand on this, the vegetation index vegindex in the development of our dynamic dust source function could be estimated by the expression:

$$\mathrm{vegindex} = 1 - A_v \quad (3)$$

$$A_v = \min\left[1.0, \min\left(V, V_t\right)/V_t\right] \quad (4)$$

where V is the parameter to describe vegetation cover. V_t is the threshold value for complete suppression of dust emissions, and A_v indicates the fraction of the area without dust emissions. In contrast to Zender's model, our study utilizes NDVI values with a resolution of 0.05° × 0.05° from the MOD13C2 version 6.1 monthly product (Didan, 2021) instead of the Leaf Area Index (LAI). This data set of NDVI, widely employed for assessing the

impact of vegetation on dust sources and for vegetation parameterization with spatial and temporal continuity (Y. Chen et al., 2023; Kim et al., 2013; Solomos et al., 2019), provides the vegetation indices used in our analysis. The summary of each utilized data set is provided in Table S1 of Supporting Information S1. For the vegetation index threshold, previous studies have suggested NDVI threshold values ranging from 0.1 to 0.17 (Y. Chen et al., 2023; Kim, Chin, Remer, et al., 2017; Kim et al., 2013; Solomos et al., 2019). Here, we consider the threshold NDVI value to be 0.1, consistent with Solomos et al. (2019). The main dust source type in the Gobi is the permanent desert, where NDVI is almost always less than 0.1 (Kim et al., 2013; Solomos et al., 2019). Taking a value of 0.1 not only limits the area of dust emissions but also characterizes the influence of vegetation both in permanent desert and seasonal active dust sources.

Previous studies have shown that early snowmelt heightens the likelihood of severe dust events, while the snow cover can inhibit dust emissions (Kurosaki & Mikami, 2004; Yin et al., 2022). However, most models do not include the parameterization of snow (J.-H. Lee & Lee, 2022). Some models simply consider the ground above a certain elevation as snow and ice-covered, unable to produce dust emissions (Zhang et al., 2024). Tanaka et al. (2011) proposed a parameterization in which the dust emission flux is linearly reduced based on the areal fraction of snow cover. We have adopted this method to account for the influence of snow cover on dust emissions, expressed as:

$$\text{snowindex} = 1 - \text{SNOWC} \tag{5}$$

here, the monthly snow fraction SNOWC (%) at a 0.05° resolution is derived from the MOD10CM version 6.1 product (Hall & Riggs, 2021b). We parameterized snow using a relatively high-resolution data set that more accurately reflects dust emissions from snow-covered areas.

Additionally, dust emissions are constrained by land cover and land use, with the primary sources being bare lands and grasslands, while other land cover type areas such as croplands only have limited contributions (C. Wu et al., 2022). The land cover type product, MCD12C1 version 6.1, provides 17 land use categories at a 0.05° spatial resolution with annual updates (Friedl & Sulla-Menashe, 2022). We assume that dust emissions could only occur under the Barren or Sparsely Vegetated land cover type and Grasslands land cover type, and we use the data set from 2021. The land use index landuseindex can be calculated as follows:

$$\text{landuseindex} = \begin{cases} 1, \text{Land use type equivalent to Barren or Sparsely Vegetated or Grasslands} \\ 0, \text{Else land use types} \end{cases} \tag{6}$$

In line with Ginoux et al.'s methodology (Equation 2), we use the Shuttle Radar Topography Mission product at 30 geographic arcseconds (~1 km) (SRTM30_Plus) (Becker et al., 2009; Farr et al., 2007; W. H. Smith & Sandwell, 1997) and consider the landuseindex to develop an elevation-based dust source function with the following equation:

$$\text{EROD}_{\text{TOPO}} = \left(\frac{z_{\max} - z}{z_{\max} - z_{\min}}\right)^5 \times \text{landuseindex} \tag{7}$$

We interpolate this data to 0.1° × 0.1° to build the erodibility $\text{EROD}_{\text{TOPO}}$ with higher resolution compared to the original $\text{EROD}_{\text{ORIG}}$ (0.25° × 0.25°). The $\text{EROD}_{\text{TOPO}}$ is expressed as a percentage (%), and like $\text{EROD}_{\text{ORIG}}$, it is structured as a three-layer variable.

Considering the combined influence of topography, vegetation, snow cover, and land use type on dust emissions, we calculate the dynamic erodibility, $\text{EROD}_{\text{MODIF}}$, using the following equation based on the methodology of previous studies (Kim et al., 2013; Tegen et al., 2002; Zender et al., 2003):

$$\text{EROD}_{\text{MODIF}} = \text{EROD}_{\text{TOPO}} \times \text{vegindex} \times \text{snowindex} \tag{8}$$

To compare the effects of vegetation and snow on dust emissions, we developed other two dust source functions, EROD_{VEG} ($\text{EROD}_{\text{VEG}} = \text{EROD}_{\text{TOPO}} \times \text{vegindex}$) and $\text{EROD}_{\text{SNOW}}$ ($\text{EROD}_{\text{SNOW}} = \text{EROD}_{\text{TOPO}} \times$ snowindex), which respectively incorporate the vegetation and snow indices. The specific descriptions of

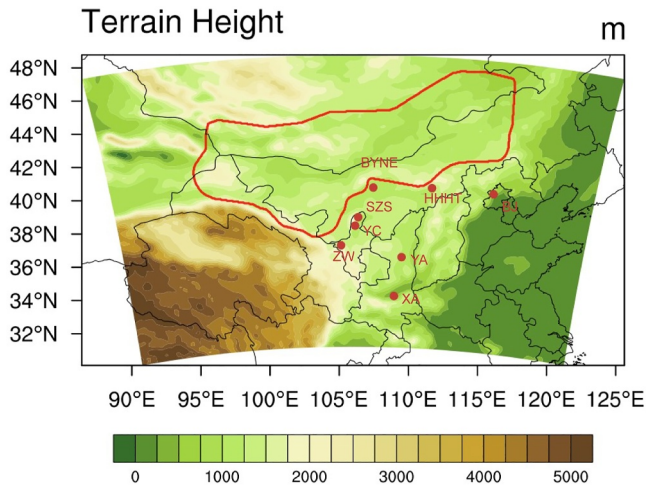

Figure 1. Overview of the WRF domain configuration and topographic features. Red dots represent observational stations for PM_{10} (ZW, Zhongwei; YC, Yinchuan; SZW, Shizuishan; BYNE, Bayannaoer; HHHT, Huhehaote; YA, Yanan; XA, Xi'an; BJ, Beijing). The red polygon outlines the geographic extent of the Gobi Desert.

different ERODs can be referred to in Table S2 of Supporting Information S1. Additionally, we exclude unrealistic dust sources near the Bohai Sea and those with EROD values less than 1E−4 (negligible impact). We calculate indexes at a raw resolution of 0.05° × 0.05° and then average the values over the 0.1° × 0.1° grid cells to obtain final indexes.

2.2. WRF-Chem Model Configuration

WRF-Chem version 4.4.1 is used for simulations in this study. The modeling domain covers the entire Gobi Desert, its surrounding regions, and parts of eastern China, capturing the primary dust sources and the major cities impacted by dust during the spring of 2023, with a grid resolution of 20 × 20 km (Figure 1). Vertically, 30 layers extend from the ground surface to the model top (50 hPa), with more levels placed in the lower troposphere to better describe boundary layer processes. To investigate the variations in dust concentrations and dust sources, simulations are conducted from 1 February 2023 to 31 May 2023. Each run covers 96 hr with a 24-hr spinup time. The outputs from previous runs are used as the initial and boundary conditions for the next run. The initial and boundary conditions of meteorological variables are from ERA5 reanalysis data with a 0.25° × 0.25° spatial resolution, updating every 6 hr. Furthermore, grid nudging is employed in all simulations to constrain meteorological conditions, ensuring consistency with observations at 6-hr intervals.

For all simulations, physical and chemical parameterization schemes are listed in Table 1. Anthropogenic emissions are derived from MIX Asian emission inventory database in 2017, covering major pollutants such as CO (carbon monoxide), SO_2 (Sulfur dioxide), NO_x (nitrogen oxides), PM_{10} (particulate matter with diameter less than or equal to 10 μm), $PM_{2.5}$ (particulate matter with diameter less than or equal to 2.5 μm), BC (black carbon), and OC (organic carbon) (M. Li et al., 2017). Biogenic emissions are calculated by the Model of Emissions of Gases and Aerosols from Nature (MEGAN) (Guenther et al., 2006).

Five experiments (ORIG, MODIF, TOPO, VEG, and SNOW) are conducted to intercompare the effects of vegetation and snow on dust and evaluate the modeling performance of the dynamic dust source function. All experiments utilize the GOCART-WRF dust emission scheme. To eliminate potential variations in meteorological conditions arising from differences in land use categories, all experiments use the land cover provided by MCD12C1 in 2021 (Friedl & Sulla-Menashe, 2022). The aerosol feedback scheme to radiation is switched off in all experiments. The ORIG experiment uses the default static dust source function $EROD_{ORIG}$, represented by the original variable EROD stored in the WRF-Chem code. The MODIF experiment uses a dynamic dust source function by replacing the original EROD in WRF with the $EROD_{MODIF}$. The TOPO, VEG, and SNOW experiments each utilize specific functions, $EROD_{TOPO}$, $EROD_{VEG}$, and $EROD_{SNOW}$, respectively. Details of each experiment are presented in Table S2 of Supporting Information S1. This study mainly focuses on the dust emission from the Gobi desert, with the region's boundaries outlined in Figure 1 using data from Natural Earth (Kelso & Patterson, 2010).

Table 1
WRF-Chem Domain Settings and Configurations for Physical/Chemical Parameterization

Domain setting	
Horizontal grid	150 × 100
Grid spacing	20 km
Vertical layers	30
Map projection	Lambert conformal
Model configuration	
Long-wave radiation	RRTMG
Short-wave radiation	RRTMG
Cumulus parameterization	Grell-Freitas ensemble scheme
Land-surface	Unified Noah land-surface model
Surface-layer	Revised MM5
Boundary layer	YSU
Microphysics	Lin et al. scheme
Chemistry scheme	RADM2 Chemistry and GOCART aerosols
Dust emission scheme	GOCART

2.3. Ground-Based and Satellite Observations

Besides the mentioned monthly data sets from MODIS (MOD13C2 and MOD10CM), we use ground-based and satellite observations from various sources, including the National Oceanic and Atmospheric Administration (NOAA), China Meteorological Administration and MODIS's Aerosol Optical Depth (AOD), to evaluate the simulation performance of the model and analyze the effects of vegetation and snow on dust storms.

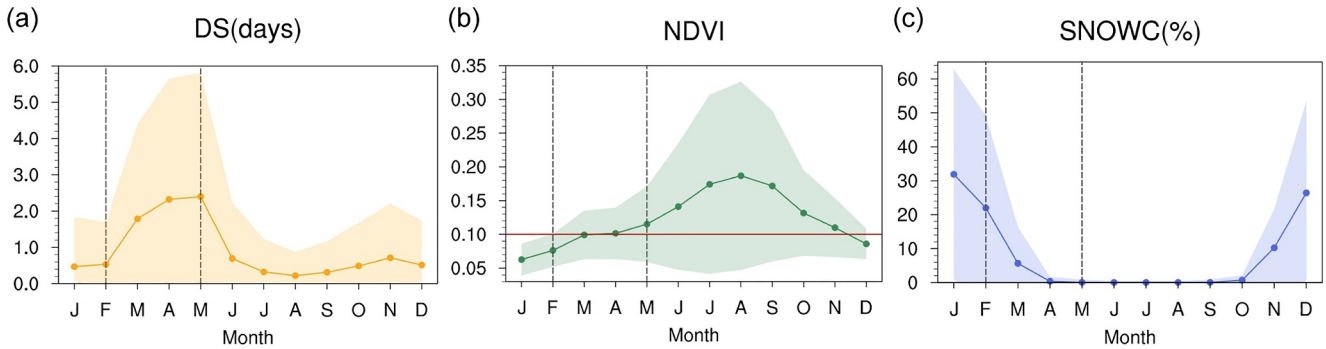

Figure 2. Monthly variations in (a) dust storm days (DS, days), (b) Normalized Difference Vegetation Index (NDVI) with the horizontal red line indicating the threshold NDVI of 0.1, and (c) snow fraction (SNOWC, %) across the Gobi region (outlined in Figure 1) from 2010 to 2023. The black dashed lines represent February and May, while the shading illustrates the interannual standard deviation.

The Integrated Surface Database (ISD) from NOAA is an archive of synchronized reports from many global surface observatories and has been used in many dust-related studies (A. Smith et al., 2011; C. Wu et al., 2022; Xi, 2021). We use dust storm records stored in the ISD data set to characterize the temporal and spatial dust activities during 2010–2023. Dust storms are defined according to World Meteorological Organization (WMO) guidelines (Codes, 1995). Weather codes 09 and 30–35 indicate the occurrence of dust storms. Any day featuring at least one record of a dust storm (09, 30–35) is defined as a dust storm day (DS). The monthly number of DS is obtained by summing the respective numbers for each month. In addition to dust, we also use data sets from ISD to validate meteorological parameters including temperature, wind speed, and relative humidity (RH).

We adopt some more quantitative dust-related variables, that is, PM_{10} and AOD, to evaluate model performance. The PM_{10} hourly concentration data used in this study are obtained from the Ministry of Ecology and Environment of China (MEE). The Retrieved Deep Blue Aerosol Optical Depth (AOD) data at a spatial resolution of $1° \times 1°$ at 550 nm is sourced from the level-3 MODIS Atmosphere Daily Global Product, version 6.1, on the Aqua and Terra platform (Platnick et al., 2015). We process daily AOD at 550 nm data (combined Dark Target and Deep Blue algorithms) of both Terra and Aqua satellites and use the average of two data for analysis.

It is noteworthy that dust storm records provide more observation locations in the studied area and a wider period compared to PM_{10} observations, with greater daily data continuity in the Gobi region than AOD data. Dust storm records have been widely used in East Asia to analyze dust occurrences and influencing factors, alongside satellite products (E.-H. Lee & Sohn, 2009; C. Wu et al., 2022; J. Wu et al., 2016). However, since the WRF-Chem model does not directly resolve dust storm events in the same manner as observational records, we utilize dust storm records to examine the spatiotemporal effects of vegetation and snow on dust storms, while employing PM_{10} concentrations and AOD data to evaluate the model performance.

3. Results

3.1. The Spatial and Temporal Variations of Dust Activities, Vegetation and Snow Cover

As one of the most prominent dust source regions in Asia, the Gobi Desert features great seasonal variability in dust storms as well as vegetation and snow. In the Gobi region, dust storms are most frequent in the spring (Figure 2a). Notably, the number of dust storm days increases dramatically after February, with more than 1.5 dust storm days per month between March and May in the period 2010–2023, and then decreases sharply after May. This monthly variation aligns with previous studies (L. Yang et al., 2021). Vegetation cover is minimal during winter, with monthly mean NDVI values below 0.1 (Figure 2b), but vegetation begins recovering rapidly in April. In February, the snow cover fraction in the Gobi can exceed 20%, while after March, the snow melts and only a small amount of snow remains in May (Figure 2c). In general, the period spanning from February to May (FMAM) in the Gobi region is marked by notable variations in dust activities, vegetation, and snow cover, with strong spring winds being the primary driver of dust storms (S. Wang et al., 2021; Xi, 2021). Nonetheless, the increase in vegetation can have an inhibiting effect on dust activities, particularly the rapid growth after April that

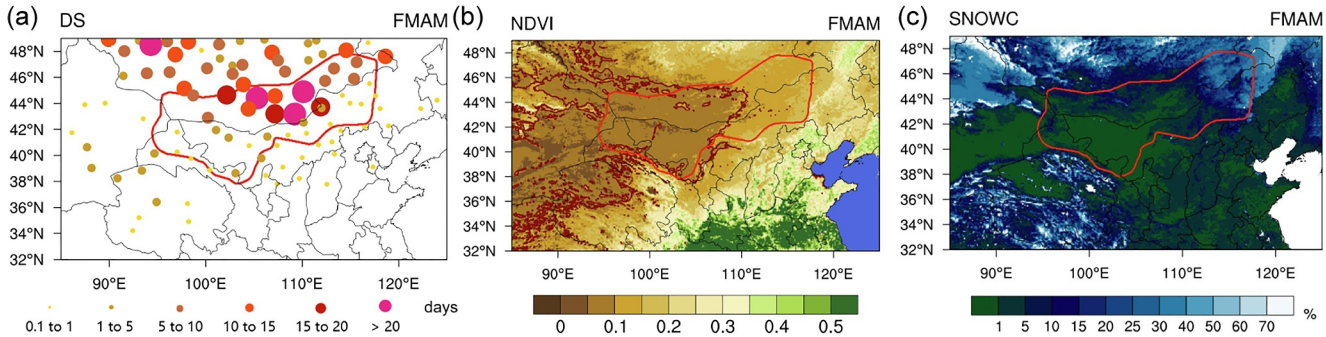

Figure 3. Spatial distributions of springtime (February – May, FMAM) averaged (a) dust storm days (DS), (b) NDVI, with barren land type subsurface indicated within the dark red line, and (c) snow fraction (SNOWC) in 2010–2023. The red polygon indicates the Gobi Desert.

can cease dust storms around June (E.-H. Lee & Sohn, 2009). Snow cover in early spring can also inhibit dust release (L. Han et al., 2011). Daily snow fraction data at a 0.05° resolution sourced from the MOD10CM version 6.1 product (Hall & Riggs, 2021a) reveals that snow cover is substantial in early February but diminishes rapidly by March, exhibiting notable daily variations (Figure S2 in Supporting Information S1). By early March, there is an increase in dust storm occurrences coinciding with relatively low snow cover. Throughout April and May, snow cover substantially decreases within the Gobi Desert, thereby alleviating its inhibitory effect on dust storms. However, it is noteworthy that severe dust storms are primarily driven by episodic strong winds (Y. Liu et al., 2022; Tai et al., 2021). Therefore, the daily variations in snow may not markedly influence the occurrence of severe dust storms, and we choose the monthly data sets to build a new dynamic dust function.

Within the Gobi Desert from February to May, dust storm days can exceed 20 days and mainly occur in Mongolia (Figure 3a). In regions characterized by frequent dust storms, NDVI values generally range from 0 to 0.15, with areas having NDVI values below 0.1 identified as major sources (S. Wang et al., 2021), aligning with the distribution of desert land types (Figure 3b). Vegetated deserts, such as the Tengger Desert, the Hunsandak Desert, and the Horqin Desert (Figure S1 in Supporting Information S1), located in Inner Mongolia, China, are not considered to be major dust sources (X. Wang et al., 2008). The southern and eastern parts of the Gobi Desert are susceptible to vegetation regrowth, and NDVI can be as high as 0.25 in some areas in May (Figures S3e and S3f in Supporting Information S1). Stations to the south of the Gobi record fewer dust storm days, and almost none in May (Figures S3a–S3d in Supporting Information S1). Several studies found that dust storms are less likely to occur in areas with high vegetation cover (Engelstaedter et al., 2003; Kimura et al., 2009; E.-H. Lee & Sohn, 2009; Zou & Zhai, 2004). Thus, the shift of dust storm activity to the south can be attributed to increased vegetation.

The average snow cover from February to May shows higher levels in the north and east (Figure 3c). Dust storm occurrences among stations in northern Gobi and to the north of Gobi show a distinct pattern: few stations record dust storm days in February, whereas records increased notably in May (Figures S3a–S3d in Supporting Information S1). Correspondingly, the average snow cover from February to May shows higher levels in the north (Figure 3c) and it shows a pronounced discrepancy from February to May. Snow cover fraction levels occasionally surpass 70% in February, while there is almost no snow cover in the Gobi region in May (Figures S3i–S3l in Supporting Information S1). Reports indicate that the wind speed threshold for dust emission under a frozen surface increases (L. Han et al., 2011) and reduced snow cover enhances the probability of dust storm outbreaks (J. Wu et al., 2016). Thus, the rise in dust storm frequency in the Northern Gobi can be attributed to the decrease in snow cover.

From 2010 to 2023, dust storms are more likely when the average (from February to May) NDVI ranges between 0.04 and 0.12, whereas they become less frequent when the NDVI surpasses 0.2 (Figure 4). The number of dust storm days increases notably when the NDVI dips below 0.11. These findings are consistent with previous studies (Dulam Jugder et al., 2014). Monthly NDVI also shows that dust storm days are more common when the monthly average NDVI is around 0.1 (Figure S4 in Supporting Information S1). Our study suggests an NDVI threshold of 0.1 for the development of long-term dynamic dust sources, which would produce strong constraints on

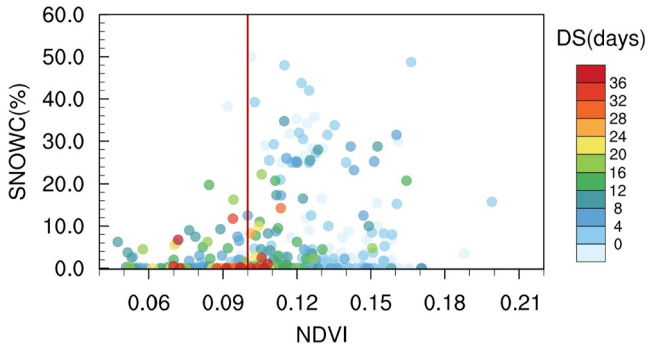

Figure 4. The relationship between NDVI, snow fraction (SNOWC), and dust storm days (DS) in the Gobi Desert: the x-coordinate of each point represents the annual average NDVI from February to May (2010–2023) for a recording station, the y-coordinate represents the annual average SNOWC from February to May (2010–2023) for the same station, and the color of each point indicates the total number of dust storm days from February to May in a specific year for that location.

simulations of dust emission. In the Gobi region, dust storm days notably increase from February to May when snow cover is below 20%, and decrease when it exceeds 50% (Figure 4). Monthly snow cover exhibits considerable variations, with April and May featuring less than 10% snow cover (Figure S4 in Supporting Information S1). While Tanaka et al. (2011) found the effects of snow cover and soil moisture on the dust event in May were very small through sensitivity studies, snow plays a limited role in dust suppression after April.

We assess the variability of dust storms, vegetation, and snow using the coefficient of variation (CV) and the standard deviation (STD), highlighting both interannual and monthly variations (Figure 5, Table 2). March and February have the largest annual variation in dust storms, with a CV of approximately 0.5, while May has the lowest (Figure 5a, Table 2). Vegetation also displays greater variability in February, similar to dust storms (Figure 5b, Table 2). Annual snow cover variability is higher in April and May (Figure 5c, Table 2). Sites are considered more variable if their annual standard deviation between February and May exceeds the median level of all sites within the Gobi Desert (Figure 5d). Overall, relatively large annual variations in dust storms occur mainly in the Gobi region of Mongolia. Substantial variations in vegetation manifest in the eastern and northern regions of the Gobi Desert, corresponding to areas of high dust storm variability. Snow, like dust storms and vegetation, also shows large interannual variations in the northern Gobi Desert. In general, the northern part of the Gobi Desert has exhibited notable variations in dust storm occurrences, vegetation, and snow cover. The occurrence of dust storms is linked to Mongolian cyclones and cold fronts, while vegetation and snow cover are influenced by precipitation (including snowfall) and temperature (Xi, 2021). With changes in weather and climate, the Mongolian Gobi has greater

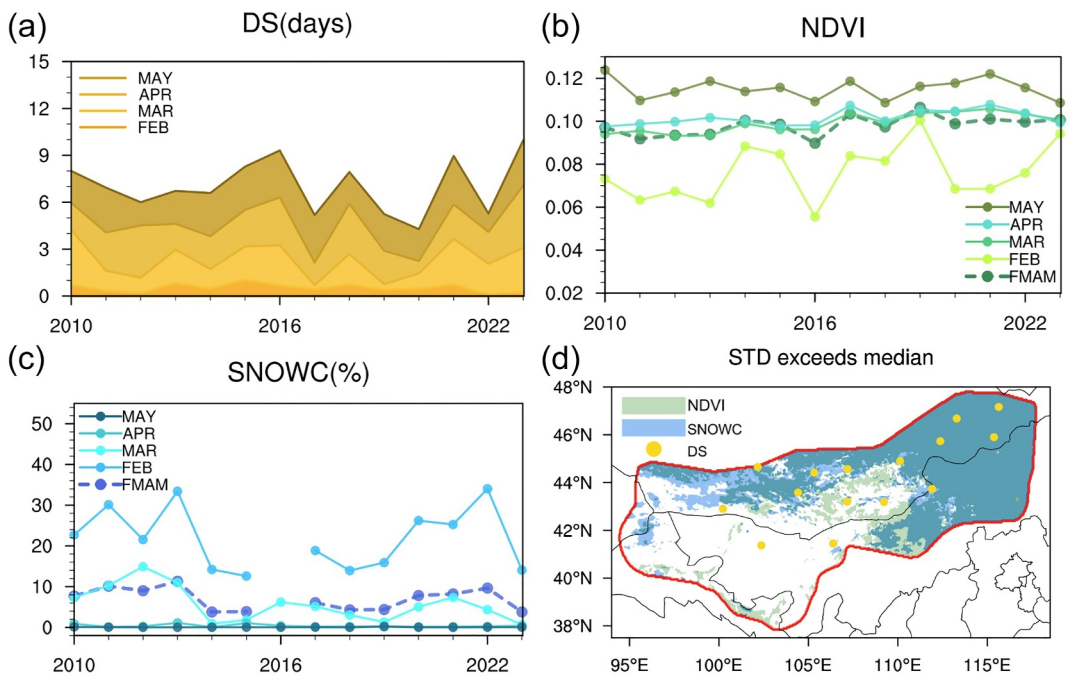

Figure 5. Annual changes in 2010–2023 of (a) dust storm days (DS), (b) NDVI, and (c) snow fraction (SNOWC) from February to May (FMAM) in the Gobi Desert. (d) Spatial distribution of high annual variability in FMAM average NDVI, SNOWC, and dust storm days (DS). Green highlights areas with high annual variability in NDVI, where the annual standard deviation (STD) exceeds the median of the 2010–2023 average annual STD for the Gobi Desert. Blue highlights areas with high annual variability in SNOWC, while yellow dots denote locations with high annual variability in DS. The criteria for identifying high variability in DS and SNOWC are consistent with those used for NDVI.

Table 2
Mean Annual Coefficients of Variation (CV) for Dust Storm Days (DS), NDVI, and Snow Fraction (SNOWC) for Each Month (February, March, April, and May) in 2010–2023

	DS	NDVI	SNOWC
		Annual CV	
FEB	0.49	0.17	0.35
MAR	0.55	0.05	0.74
APR	0.36	0.03	0.92
MAY	0.25	0.04	0.92

annual variability than other Gobi areas, mainly in the formation of greater variability in surface features and dust activities. In turn, the interannual variability of surface features can have a temporal impact on dust activities.

The dominant factor in decreasing dust storms in East Asia in recent years was a decrease in wind speeds (Tai et al., 2021; C. Wu et al., 2022). However, unusually severe dust storms originating from the Gobi Desert occurred in the springs of 2021 to 2023. The spring of 2023 marked most dust storm events in the Gobi Desert (S. Chen et al., 2023), albeit less severe than the super dust storm of March 2021. Vegetation and snow cover levels during spring were higher in 2021 than in 2023 (Figures 5b and 5c), suggesting less favorable surface conditions for dust emissions in 2021. Considering the representativeness of the model evaluation, we favor the spring of 2023, when dust storms were more frequent and more responsive to changes in the land surface.

3.2. Dynamic Representation of Dust Sources and the Key Influencing Factors on Dust Emissions

Figures 6a and 6b illustrate the spatial distribution of the initial dust source function ($EROD_{ORIG}$; the original erodibility) and the averaged dynamic dust source function ($EROD_{MODIF}$; the dynamic erodibility) for February to May in 2023. The spatial distributions of the two erodibilities are similar and both capture the major dust sources in the Gobi Desert region, including the main dust sources in China and southern Mongolia, predominantly categorized as desert land use type (X. Wang et al., 2008). Compared to the original erodibility, the dynamic erodibility reduces the intensity of the erodibility in the southern Gobi Desert by up to 30% (absolute

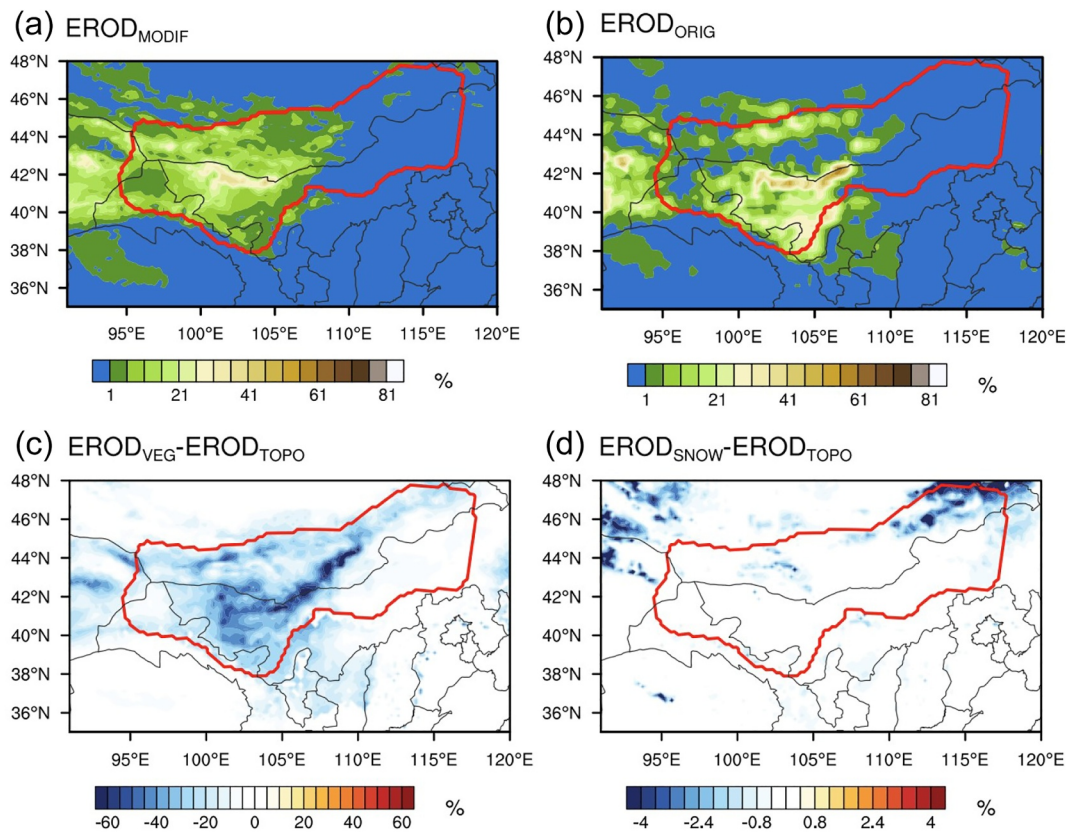

Figure 6. Spatial distributions of springtime (February – May, FMAM) averaged (a) $EROD_{ORIG}$ (the erodibility from the ORIG experiment), (b) $EROD_{MODIF}$ (the erodibility from the MODIF experiment), (c) the effect of vegetation on erodibility (the differences between $EROD_{VEG}$ and $EROD_{TOPO}$), and (d) the effect of snow on erodibility (the differences between $EROD_{SNOW}$ and $EROD_{TOPO}$).

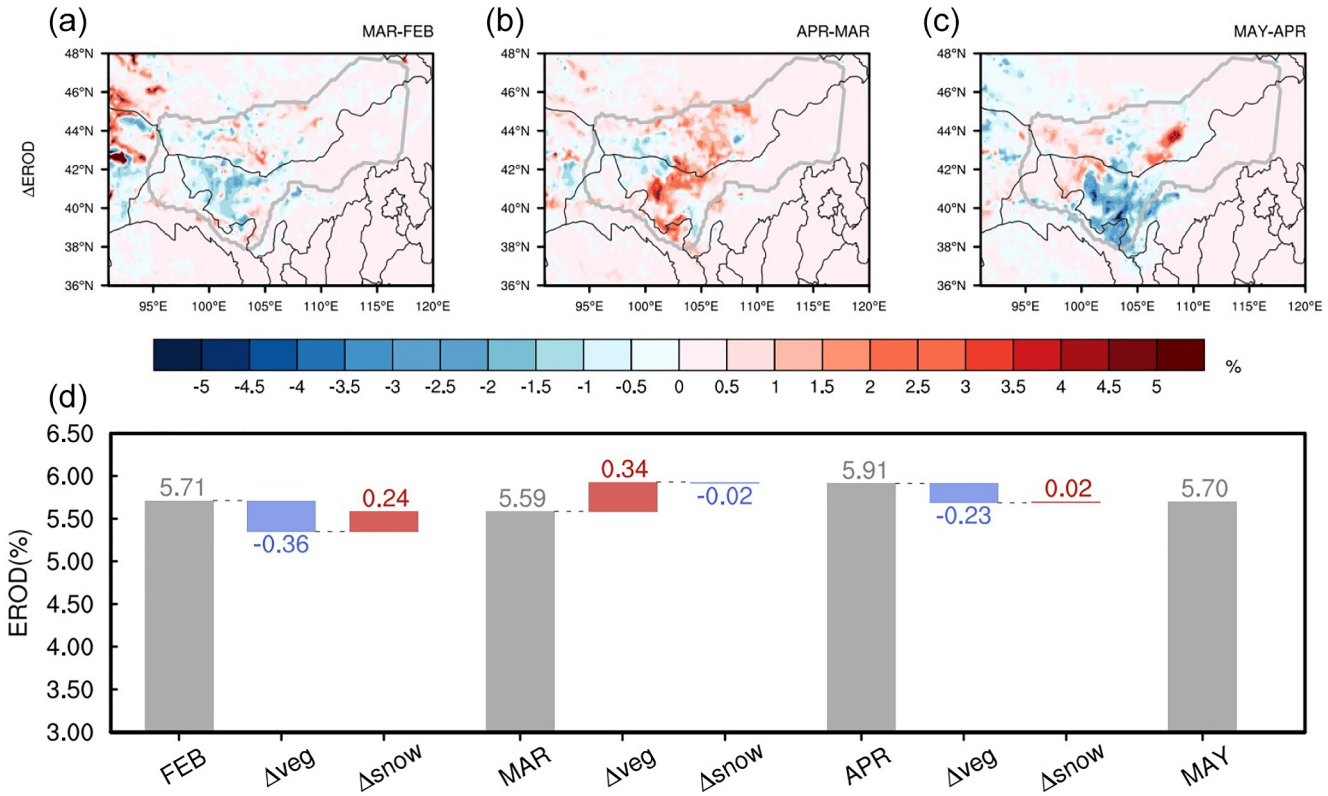

Figure 7. Spatial distributions of absolute changes (%) in $EROD_{MODIF}$ between (a) March and February, (b) April and March, and (c) May and April. The gray polygon indicates the Gobi Desert. (d) Averaged $EROD_{MODIF}$ (gray squares, unit:%) for February, March, April, and May. Changes in erodibility due to differences in vegetation index and snow index (Δveg and Δsnow) between 2 months (blue squares indicate negative effects, red squares indicate positive effects).

change) and enhances the intensity of the erodibility in southern Mongolia by about 20% (Figure S5 in Supporting Information S1). We quantify the erodibility magnitude over the Gobi region, finding that the overall values of the original erodibility and the dynamic erodibility are nearly equivalent, with average values of 6.33% and 5.73%, respectively.

Higher resolution data sets enhance the accuracy of dust source function calculations by capturing minor topographic differences within the same region, as well as resulting in relatively higher values of erodibility. $EROD_{TOPO}$ (erodibility without considering vegetation and snow indexes) proves more adept at capturing the intricacies of troughs and depressions within the Gobi Desert, encompassing dust sources within the Alashan Plateau in China, the Great Lakes Depression in Mongolia, and the region south of the Altai Mountains in Mongolia (Figure 6a), which is more consistent with observations (D. Jugder et al., 2018; X. Wang et al., 2008). The combined inhibitory effects of vegetation and snow amount to roughly 20%, yielding a slightly smaller dynamic erodibility than the original erodibility on average from February to May (Figures 6c and 6d). The inhibitory effect of vegetation is notably greater than that of snow, reducing erodibility in the Gobi Desert, particularly near the China-Mongolia border, where erodibility is relatively high, by approximately 60%. In comparison, the inhibitory of snow is more pronounced in areas with higher snow cover, reducing erodibility by approximately 4% in the northern and eastern–northern parts of the Gobi Desert.

In February, the average dynamic erodibility in the Gobi Desert was 5.71%, slightly higher than the value of March, which was 5.59% (Figure 7d). Rising temperatures in March reduced snow fraction exceeding 20% in southern Mongolia (Figure S6d in Supporting Information S1), as indicated by an approximate 0.3 increase in the snow index (Figure S7d in Supporting Information S1), leading to a rise of 0.24% in the mean dynamic erodibility for the Gobi Desert (Figure 7d). At the same time, vegetation recovery in the southern region of the Gobi reduced the vegetation index (Figures S6a and S7a in Supporting Information S1), decreasing the dynamic erodibility by 0.36% (Figure 7d). Consequently, the combined effect of vegetation and snow resulted in a lower erodibility in March compared to February. Moreover, March precipitation was nearly 50% below the average of the

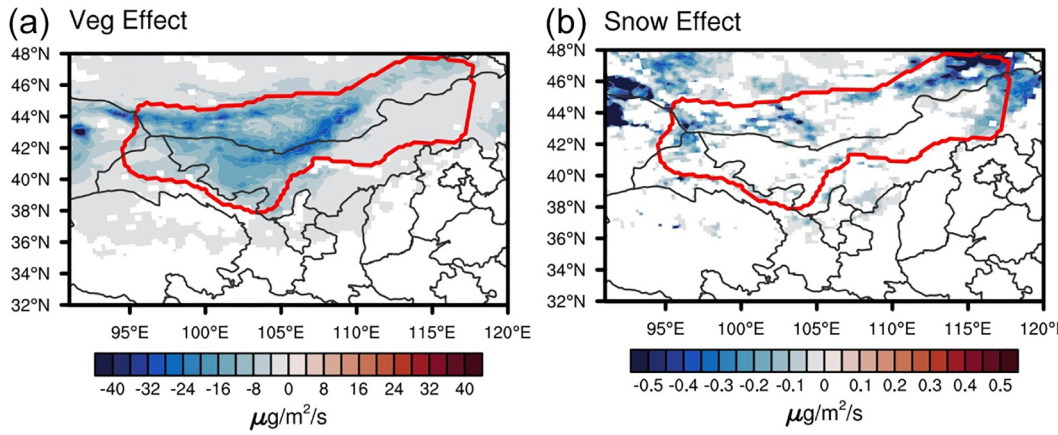

Figure 8. Spatial distributions of (a) the vegetation effect on dust emissions (μg/m^2/s) (differences between the VEG experiment and the TOPO experiment) and (b) the snow effect on dust emissions (differences between the SNOW experiment and the TOPO experiment), averaged over February to May 2023.

climatology, and warmer temperatures (Yin et al., 2023) further hindered vegetation growth. As a result, NDVI decreased in the southern part of the Gobi and the southern part of Mongolia (Figure S6b in Supporting Information S1) and the vegetation index increased (Figure S5b in Supporting Information S1), contributing to a 0.34% increase in the erodibility (Figure 7d). Conversely, there was almost no snow cover after March, with only a minor increase of approximately 10% in the western Gobi (Figure S6e in Supporting Information S1). This change in the snow index resulted in only a 0.2% change in the erodibility. Vegetation recovery at Gobi South from April to May led to an average decrease of 0.23% in the erodibility, ultimately bringing the dust source function in May to a level almost equivalent to that in February. Yin et al. (2022) suggested that more snowmelt and sparser vegetation could create favorable conditions for the emergence of dust storms. The utilization of monthly data in developing the dynamic erodibility effectively captures temporal shifts in vegetation and snow.

From February to May 2023, total dust emissions across the Gobi Desert are estimated to exceed 30 Tg, surpassing levels from previous years. Mongolia contributed approximately 42% of the dust observed in northern China during spring (S. Chen et al., 2023). However, $EROD_{ORIG}$ omitted dust sources in southern Mongolia, regions known for high dust emission rates (Jin et al., 2022; Mao et al., 2013; Tanaka et al., 2011; C. Wu et al., 2022), resulting in the ORIG experiment's less effective capture of dust emissions in this area compared to the MODIF experiment (Figure S8 in Supporting Information S1). Dust emissions are notably influenced by near-surface meteorological conditions and land surface characteristics, and vegetation and snow cover are key factors in regulating dust activity through their influence on dust emissions (Mao et al., 2013). C. Wu et al. (2022) attributed the decrease in dust storms over East Asia from 2001 to 2017 to a 30% increase in grassland vegetation. Tanaka et al. (2011) conducted sensitivity studies that indicated snow cover had a relatively small impact on reducing dust emission fluxes during the March 2007 dust event in semi-arid regions of East Asia. However, few studies have combined extensive observational or satellite data with numerical modeling to quantitatively assess the effects of vegetation and snow cover on dust emissions. To investigate the specific effects of vegetation and snow on dust emissions, sensitivity experiments were conducted employing various dust source functions. Vegetation decreases dust emissions in the low-lying regions of the Gobi Desert near the China-Mongolia border, by about 20 μg/m^2/s (Figure 8a). This finding is consistent with previous studies demonstrating the impact of vegetation on dust emissions throughout northern China, southern Mongolia, and eastern Mongolia (Mao et al., 2013; Tai et al., 2021; C. Wu et al., 2022). In comparison, the impact of snow cover is considerably smaller, decreasing emissions by only up to 0.5 μg/m^2/s (Figure 8b), primarily in the northern Gobi Desert where snow cover is comparatively abundant (J.-J. Lee & Kim, 2012; Tanaka et al., 2011). The effects of vegetation and snow on dust emissions exhibit considerable seasonal variation, as detailed in Table 3. The mitigating impact of vegetation on dust emissions is most pronounced during spring, especially in April, aligning with the annual peak in dust activity and corroborating previous research findings (Song et al., 2017; C. Wu et al., 2022). Over the period from February to May 2023, vegetation contributes to an average reduction in dust emissions of

Table 3
Changes of Monthly Averaged Dust Emission Fluxes (μg/m²/s) Averaged Across the Gobi Desert by Vegetation and Snow Indexes

	FMAM	FEB	MAR	APR	MAY
Vegetation index	−9.17	−3.07	−9.22	−13.53	−12.26
Snow index	−0.08	−0.18	−0.04	−0.05	−0.04

approximately 9.17 μg/m²/s, substantially greater than the impact of snow, which averages only about 0.08 μg/m²/s.

3.3. Application and Improvements in Dust Storm Simulation

The model performance of WRF-Chem in replicating meteorological variables (specifically, air temperature at 2-m, relative humidity, and wind speed at 10-m) through comparative analysis with observational data is shown in Table S4 of Supporting Information S1. The locations of observing stations can be referred to in Figure S1 of Supporting Information S1. The correlation coefficients (r) for 2-m air temperature consistently exceed 0.98, those for 2-m relative humidity exceed 0.9, and those for wind speed surpass 0.7. The metrics of mean bias (MB) and root-mean-square error (RMSE) are all small values. Hence, the model generally reproduces meteorological conditions within an acceptable range of accuracy.

In this study, we compare and analyze the spatial distributions and temporal variations of AOD from MODIS and simulations during February– May 2023. Typically, MODIS-derived AOD values are higher than those obtained from model simulations; therefore, direct comparisons of absolute AOD are often avoided (L. Liu et al., 2016; F. Wang et al., 2022; S. Yang et al., 2021). The MODIS results show that high AODs are mainly concentrated in the southern and western parts of the Gobi Desert, with average AOD reaching up to 0.4 (Figure 9a), indicating that the dust concentrations are relatively high in these two regions. The spatial distribution patterns in both experiments are comparable to MODIS and they replicate high AOD over the Gobi Desert (Figures 9a and 9b). S. Chen et al. (2023) reported that the number of dust storms in North China rose markedly in the spring of 2023, with dust during March and April primarily originating from Mongolia, especially the western Gobi. The MODIF experiment shows higher AOD values in southern Mongolia near the China border compared to the ORIG experiment, aligning more closely with the MODIS distribution. Conversely, the erodibility of the MODIF experiment in the southern part of the Gobi is reduced, resulting in a lower AOD. Since ground-based PM_{10} data provide comprehensive daily measurements and are better suited for validating models in urban areas, we selected AOD data to validate the dust model in regions with low anthropogenic emissions, specifically the western Gobi

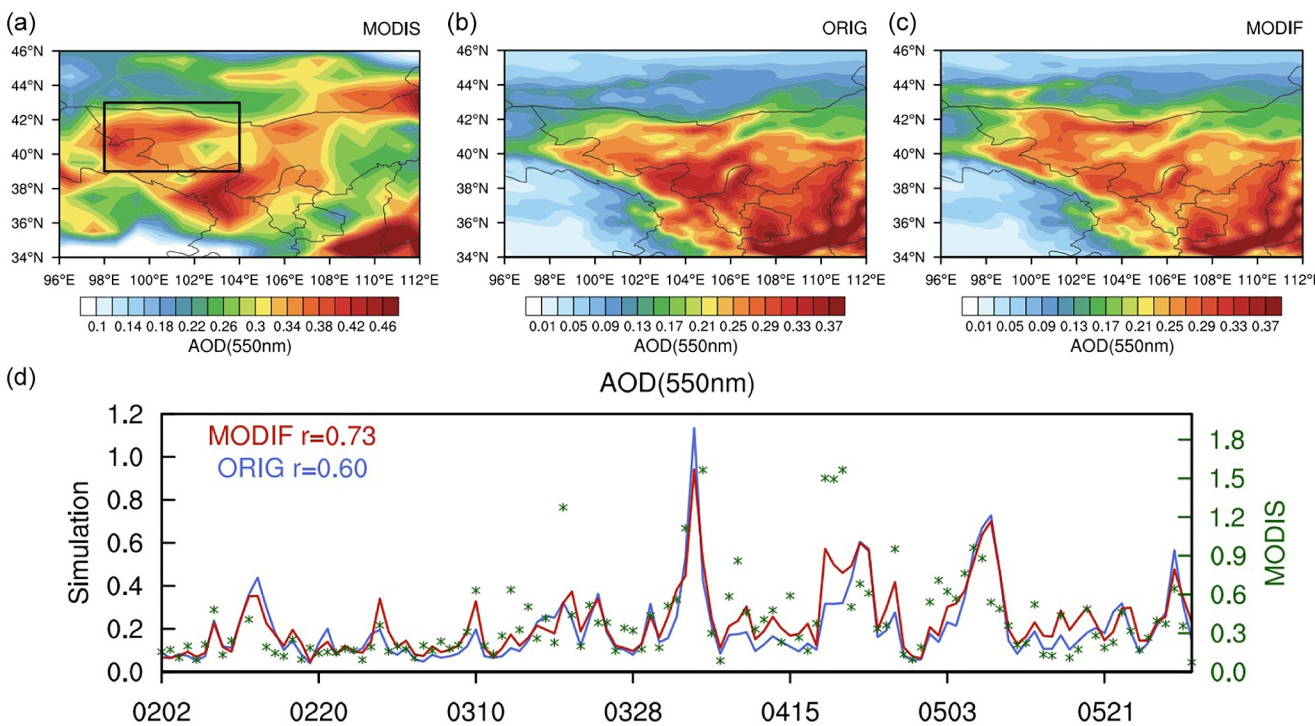

Figure 9. Spatial distributions of averaged AOD based on (a) MODIS (the black rectangle indicates the location of the western part of the Gobi Desert), WRF-Chem simulations of (b) the ORIG experiment and (c) the MODIF experiment during February–May 2023. (d) Daily variations of AOD from MODIS (in green stars), the ORIG experiment (in blue line) and the MODIF experiment (in red line) within the black rectangle in (a).

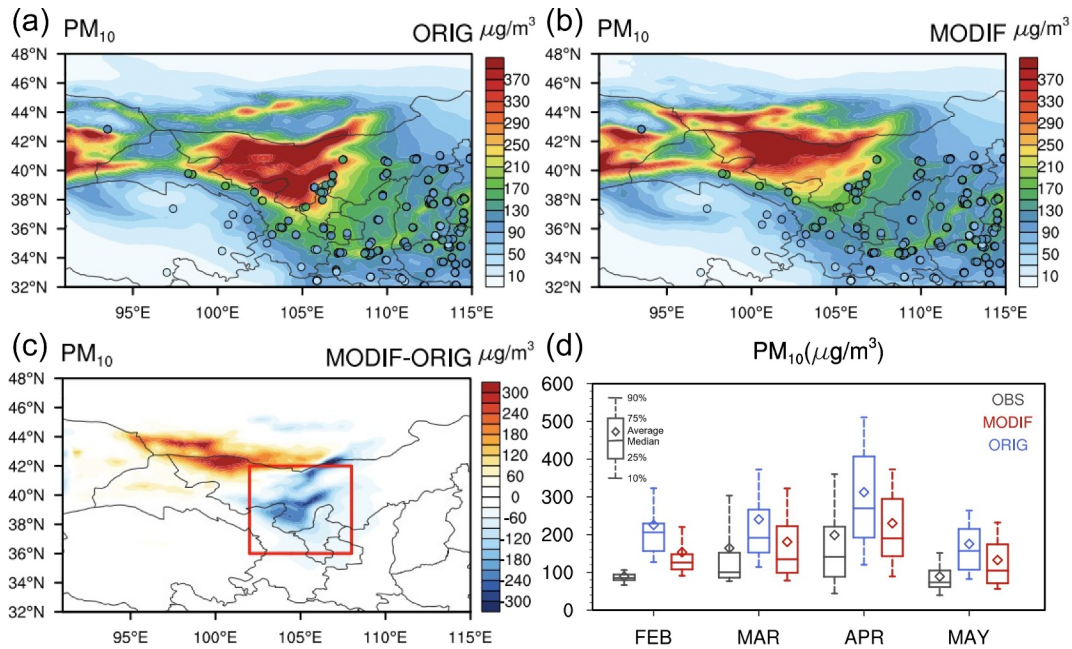

Figure 10. Spatial distributions of averaged PM_{10} concentrations of (a) the ORIG experiment, (b) the MODIF experiment (colored dots indicating observed PM_{10} concentrations), and (c) the difference between MODIF and ORIG. The red rectangle indicates the location of cities near dust sources. (d) Monthly PM_{10} concentrations of OBS (observation), MODIF and ORIG experiments of cities near dust sources.

Desert (within the black rectangle in Figure 9a). We find that the correlation between the two sets of experiments and MODIS is quite good, with correlation coefficients (r) exceeding 0.60 (Figure 8d), which indicates that the model can simulate the daily variation of dust well. However, the r of the MODIF experiment reaches 0.73, better than the ORIG experiment (both experiments pass the significance test of $p < 0.05$). As a result, the dynamic erodibility can more accurately represent AOD in the western part of the Gobi Desert. Previous studies have also reported high AOD values in the Chinese Alashan Plateau near the China-Mongolia border (Ginoux et al., 2012; M. Tao et al., 2017), and dust sources in this area are categorized as natural sources. Thus, the dynamic dust source function can more accurately describe dust source distributions in the Gobi Desert.

The spatial distributions of simulated and observed PM_{10} concentrations averaged from February to May 2023 are shown in Figure 10. The ORIG experiment indicates an overestimation of PM_{10} concentrations, with values reaching approximately 290 μg/m^3 in urban areas, compared to observations (Figure 10a). The MODIF experiment does not show such an overestimation and demonstrates a closer alignment of simulated PM_{10} concentrations with observations (Figure 10b). This improved accuracy suggests that incorporating dynamic factors related to vegetation and snow substantially mitigates dust emissions in the Gobi region and provides a better representation of how alterations in surface properties impact dust activities. Additionally, the erodibility at the China-Mongolia border increases due to the replacement of a finer topographic data set, consequently elevating the modeled PM_{10} concentrations in this area (Figure 10c). The red rectangle in Figure 10c outlines the cities near dust sources in China (36°– 42°N, 102°–108°E). Figure 10d provides a comparative analysis of the monthly PM_{10} concentration variations between the two experiments in this specific area. The results prove that the dynamic erodibility can capture the temporal changes in PM_{10} concentrations more accurately than the original erodibility.

Dust storms tend to induce severe air pollution in cities situated near dust sources. PM_{10} concentrations typically spike rapidly at the onset of dust events and then decline quickly, leading to fluctuations in PM_{10} levels by a factor of two or even several orders of magnitude (Dulam Jugder et al., 2014; Filonchyk, 2022). Figure 11 shows the validation results of two experiments in four cities located near dust sources in comparison to observations. Two statistical measures, r and MB, are used to assess the simulation performance. In several cities, the MODIF experiment exhibits an improvement in the simulation of PM_{10} compared to the ORIG experiment, with r approaching or surpassing 0.6 (confirmed by a significance test at $p < 0.05$). In certain cities and months, the

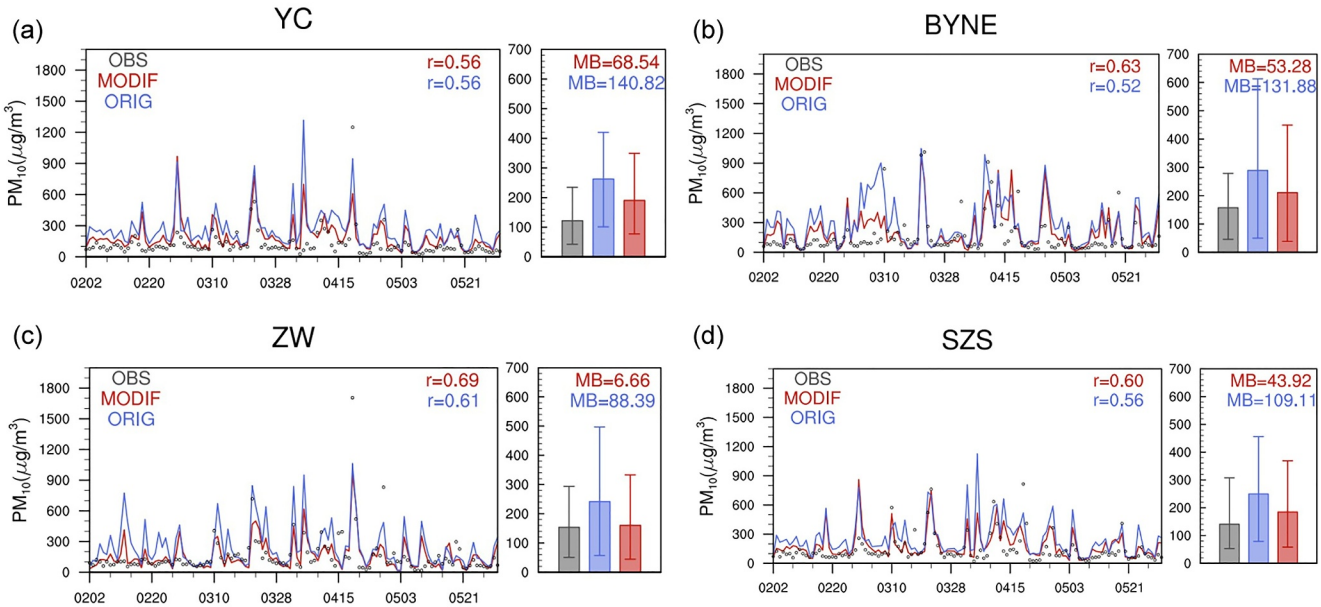

Figure 11. Simulated and observed daily PM_{10} concentration variations and average PM_{10} concentrations (the short upper line of the box indicates the upper ninth quartile, the short lower line indicates the lower ninth quartile, and the upper edge of the rectangle indicates the average) in 4 near dust sources cities (a) Yinchuan (YC), (b) Bayannaoer (BYNE), (c) Zhongwei (ZW), and (d) Shizuishan (SZS), locations are shown in Figure 1 from February to May 2023.

correlation coefficient can reach 0.9, and r and MB improve in every month in all cities (Table S5 in Supporting Information S1). It is noted that the GOCART-WRF scheme might spuriously generate dust emissions in models during very low wind conditions (LeGrand et al., 2019), potentially contributing to the overestimation of PM_{10} in the ORIG experiment. Dynamic erodibility generally corrects the overestimation of PM_{10} compared with original erodibility, which can exceed 100 μg/m^3 in some cities. In cities like Zhongwei, dynamic erodibility only results in an average MB of PM_{10} of less than 10 μg/m^3 from February to May (Figure 11). Additionally, the MODIF experiment demonstrates improvements in simulating PM_{10} concentrations in cities across northern and central China, albeit to a lesser extent compared to those near dust sources. As demonstrated in Figure S9 of Supporting Information S1, the ORIG experiment tends to overestimate PM_{10} concentrations, whereas MODIF partially mitigates this issue. Despite the closer alignment of PM_{10} concentrations simulated by the MODIF model, the enhancements in correlation coefficients (r) are relatively modest. This could be attributed to the influence of anthropogenic activities on PM_{10} levels in these urban areas, particularly in densely populated and heavily polluted regions (Ding et al., 2017). Our findings suggest that the default GOCART-WRF scheme tends to simulate spurious dust emissions and overestimate particulate matter concentrations. In contrast, the dynamic dust source function provides a more accurate reflection of the impacts of vegetation and snow on dust activity by considering their roles in reducing dust emissions. This contributes to enhanced spatial and temporal modeling of dust activity.

4. Conclusions

This study examines the variations of vegetation, snow, and dust storms in the Gobi Desert and their interrelationships, employing multiple satellite and observational data for the past decade. To enhance the understanding of their effects on dust activities, the GOCART dust emission scheme coupled with WRF-Chem is improved by adopting a novel parameterization method with satellite observations. The development of the dust source function integrates high-resolution topographic data specific to the Gobi region, along with factors of vegetation and snow. Numerical simulations were conducted from February to May 2023, with monthly changes in vegetation and snow informing the spatiotemporal dynamics of dust sources. The individual effects of vegetation and snow on both the dust source function and dust emissions were analyzed. The simulation results illustrate that the dynamic dust source function in the Gobi Desert performs better in capturing dust sources and simulating dust activities.

In the Gobi Desert, there are notable variations in dust storms, vegetation and snow cover from February to May. During this period, dust storms are getting frequent, vegetation is sparse, and snow cover is minimal. There is a relationship between vegetation, snow, and dust storms. As vegetation begins to flourish and snow gradually melts from February through May, the occurrence and intensity of dust storms undergo notable shifts. Strong dust storms are more likely to occur when NDVI is less than about 0.1, and snow cover is less than 20%. It is noteworthy that the Gobi Desert, particularly the Mongolian Gobi, exhibits interannual and seasonal variations in vegetation, snow cover and dust storms.

We develop a new dynamic dust source function, which considers both vegetation and snow parameters, utilizing high-resolution topographic data. This enhancement increases the intensity of the dust source function in the southern region of Mongolia and diminishes it in the southern parts of the Gobi Desert. The influence of vegetation is considerably more pronounced and widespread compared to snow, which has a relatively minor effect, primarily influencing dust sources in the northern Gobi. Additionally, monthly variations in dust sources are predominantly driven by alterations in vegetation.

Through five numerical experiments and a comparative analysis of the simulation results, we underscore the crucial role of vegetation and snow cover in governing dust emissions. By quantitatively assessing their individual effects on dust emissions, we enhance our understanding of their contributions to dust activities. During spring, vegetation emerges as a pivotal factor in mitigating dust emissions, particularly in April, when dust emission levels are relatively high. Vegetation notably reduces dust emissions in the low-lying areas of the Gobi Desert near the China-Mongolia border, where dust emissions are high. In contrast, snow cover plays a lesser role in dust reduction, especially post-February, predominantly impacting the northern Gobi Desert.

The development of dynamic dust source functions has enhanced the simulation performance in numerous studies. We observe that the dynamic dust source function can better represent AOD in the western part of the Gobi Desert, along the China-Mongolia border. For Chinese cities, this improved dynamic dust source function yields notable improvements in PM_{10} simulation during the springtime (from February to May). The enhancements are evidenced by increased correlation coefficients and notably decreased mean biases. Moreover, this function provides a more precise depiction of the monthly fluctuations in PM_{10} levels. It is worth noting that the dynamic dust source function corrects the bias in spurious dust emission in the GOCART-WRF scheme.

Nonetheless, this study raises additional points for discussion. According to our evaluation of aerosol optical thickness simulation, we discover that both the original and dynamic dust source functions are unable to accurately capture dust emissions in regions such as the Hunsandak Desert and the Horqin Desert in Inner Mongolia, which are affected by vegetation and human activity and are believed to be anthropogenic dust sources rather than major dust sources (Ginoux et al., 2012; X. Wang et al., 2008). Further investigation into the impact of dynamic factors on dust is warranted. Additionally, the 0.1 vegetation threshold established in our study has proven effective for dust modeling in the Gobi Desert. However, global dust models generally use a uniform threshold for vegetation parameterization, and it is not yet clear if this threshold is applicable to most deserts around the world. In summary, this research utilizes multiple observational and modeling approaches to study the impact of vegetation and snow on dust activities, offering valuable insights into the effects of vegetation and snow on dust storms over the Gobi Desert, as well as parametric representations of time-varying dust sources.

Data Availability Statement

The source code of the WRF-Chem model is archived at https://github.com/wrf-model/WRF/releases/tag/v4.4.1. Terrain height data from SRTM are accessible at https://topex.ucsd.edu/pub/srtm30_plus/srtm30/grd/. Monthly NDVI data sets, MOD13C2, are available at https://ladsweb.modaps.eosdis.nasa.gov/archive/allData/61/MOD13C2, and monthly snow fraction data sets, MOD10CM, can be downloaded from https://nsidc.org/data/data-access-tool/MOD10CM/versions/61. Daily snow fraction data sets, MOD10C1, can be downloaded from https://nsidc.org/data/data-access-tool/MOD10C1/versions/61. Annual land use data sets (MCD12C1) can be found at https://ladsweb.modaps.eosdis.nasa.gov/archive/allData/61/MCD12C1. Daily AOD data sets from MOD08_D3 and MYD08_D3 are accessible at https://ladsweb.modaps.eosdis.nasa.gov/archive/allData/61/MOD08_D3 and https://ladsweb.modaps.eosdis.nasa.gov/archive/allData/61/MYD08_D3, respectively. Hourly PM_{10} data sets, courtesy of the Ministry of Ecology and Environment of China (MEE), are available at https://www.aqistudy.cn/historydata/. Data sets on dust recording and weather observations generated from ISD are accessible at ftp://ftp.

ncdc.noaa.gov/pub/data/noaa/. The shapefile data containing information on the Gobi Desert can be obtained from https://www.naturalearthdata.com/downloads/50m-physical-vectors/50m-physical-labels/. All data sets contained in the paper are available upon reasonable request.

Acknowledgments
This work was supported by the National Natural Science Foundation of China (42325506), the Fundamental Research Funds for the Central Universities (14380198), and the Second Tibetan Plateau Scientific Expedition and Research (STEP) program (2019QZKK0106).

References

Abdourhamane Touré, A., Tidjani, A. D., Rajot, J. L., Marticorena, B., Bergametti, G., Bouet, C., et al. (2019). Dynamics of wind erosion and impact of vegetation cover and land use in the Sahel: A case study on sandy dunes in Southeastern Niger. *Catena*, *177*, 272–285. https://doi.org/10.1016/j.catena.2019.02.011

Albani, S., Mahowald, N. M., Perry, A. T., Scanza, R. A., Zender, C. S., Heavens, N. G., et al. (2014). Improved dust representation in the community atmosphere model. *Journal of Advances in Modeling Earth Systems*, *6*(3), 541–570. https://doi.org/10.1002/2013MS000279

Becker, J. J., Sandwell, D. T., Smith, W. H. F., Braud, J., Binder, B., Depner, J. L., et al. (2009). Global bathymetry and elevation data at 30 arc seconds resolution: SRTM30_PLUS. *Marine Geodesy*, *32*(4), 355–371. https://doi.org/10.1080/01490410903297766

Bran, S. H., Macatangay, R., Surapipith, V., Chotamonsak, C., Chantara, S., Han, Z., & Li, J. (2022). Surface $PM_{2.5}$ mass concentrations during the dry season over northern Thailand: Sensitivity to model aerosol chemical schemes and the effects on regional meteorology. *Atmospheric Research*, *277*, 106303. https://doi.org/10.1016/j.atmosres.2022.106303

Cakmur, R. V., Miller, R. L., Perlwitz, J., Geogdzhayev, I. V., Ginoux, P., Koch, D., et al. (2006). Constraining the magnitude of the global dust cycle by minimizing the difference between a model and observations. *Journal of Geophysical Research*, *111*(D6). https://doi.org/10.1029/2005JD005791

Chappell, A., Webb, N. P., Hennen, M., Zender, C. S., Ciais, P., Schepanski, K., et al. (2023). Elucidating hidden and enduring weaknesses in dust emission modeling. *Journal of Geophysical Research: Atmospheres*, *128*(17), e2023JD038584. https://doi.org/10.1029/2023JD038584

Chen, S., Zhao, D., Huang, J., He, J., Chen, Y., Chen, J., et al. (2023a). Mongolia contributed more than 42% of the dust concentrations in Northern China in March and April 2023. *Advances in Atmospheric Sciences*, *40*(9), 1549–1557. https://doi.org/10.1007/s00376-023-3062-1

Chen, Y., Zhang, Y., Chen, S., Yang, B., Yan, H., Li, J., et al. (2023b). Impacts of dynamic dust sources coupled with WRF-Chem 3.9.1 on the dust simulation over East Asia (preprint). *Atmospheric sciences*. https://doi.org/10.5194/gmd-2023-81

Chow, K.-C., Su, L., Fung, J. C. H., Ma, H., & Lau, A. K. H. (2014). Numerical modeling of a strong dust event over the South China region in March 2010. *Meteorology and Atmospheric Physics*, *126*(3), 119–138. https://doi.org/10.1007/s00703-014-0338-0

Codes, M. O. (1995). *International codes–WMO no. 306*. World Meteorological.

Didan, K. (2021). MODIS/Aqua vegetation indices monthly L3 global 0.05 deg CMG V061 [dataset]. *NASA EOSDIS Land Processes DAAC*. https://ladsweb.modaps.eosdis.nasa.gov/missions-and-measurements/products/MYD13C2

Ding, A., Huang, X., & Fu, C. (2017). Air pollution and weather interaction in East Asia. In A. Ding, X. Huang, & C. Fu (Eds.), *Oxford research encyclopedia of environmental science*. Oxford University Press. https://doi.org/10.1093/acrefore/9780199389414.013.536

Engelstaedter, S., Kohfeld, K. E., Tegen, I., & Harrison, S. P. (2003). Controls of dust emissions by vegetation and topographic depressions: An evaluation using dust storm frequency data. *Geophysical Research Letters*, *30*(6). https://doi.org/10.1029/2002GL016471

Escap, U. (2021). Sand and dust storms risk assessment in Asia and the Pacific. Retrieved from https://repository.unescap.org/handle/20.500.12870/4452

Falkowski, P., Barber, R., & Smetacek, V. (1998). Biogeochemical controls and feedbacks on ocean primary production. *Science*, *281*(5374), 200–206. https://doi.org/10.1126/science.281.5374.200

Farr, T. G., Rosen, P. A., Caro, E., Crippen, R., Duren, R., Hensley, S., et al. (2007). The shuttle radar topography mission. *Reviews of Geophysics*, *45*(2). https://doi.org/10.1029/2005rg000183

Filonchyk, M. (2022). Characteristics of the severe March 2021 Gobi Desert dust storm and its impact on air pollution in China. *Chemosphere*, *287*(Pt 3), 132219. https://doi.org/10.1016/j.chemosphere.2021.132219

Friedl, M., & Sulla-Menashe, D. (2022). MODIS/Terra+ Aqua land cover type yearly L3 global 0.05 Deg CMG V061. *NASA EOSDIS Land Processes DAAC*, *61*. https://doi.org/10.5067/MODIS/MCD12C1

Ginoux, P., Chin, M., Tegen, I., Prospero, J. M., Holben, B., Dubovik, O., & Lin, S.-J. (2001). Sources and distributions of dust aerosols simulated with the GOCART model. *Journal of Geophysical Research*, *106*(D17), 20255–20273. https://doi.org/10.1029/2000JD000053

Ginoux, P., Prospero, J. M., Gill, T. E., Hsu, N. C., & Zhao, M. (2012). Global-scale attribution of anthropogenic and natural dust sources and their emission rates based on MODIS Deep Blue aerosol products. *Reviews of Geophysics*, *50*(3). https://doi.org/10.1029/2012RG000388

Ginoux, P., Prospero, J. M., Torres, O., & Chin, M. (2004). Long-term simulation of global dust distribution with the GOCART model: Correlation with North Atlantic oscillation. *Environmental Modelling & Software*, *19*(2), 113–128. https://doi.org/10.1016/S1364-8152(03)00114-2

Grini, A., Myhre, G., Zender, C. S., & Isaksen, I. S. A. (2005). Model simulations of dust sources and transport in the global atmosphere: Effects of soil Erodibility and wind speed variability. *Journal of Geophysical Research*, *110*(D2). https://doi.org/10.1029/2004JD005037

Guenther, A., Karl, T., Harley, P., Wiedinmyer, C., Palmer, P. I., & Geron, C. (2006). Estimates of global terrestrial isoprene emissions using MEGAN (model of emissions of Gases and Aerosols from nature). *Atmospheric Chemistry and Physics*, *6*(11), 3181–3210. https://doi.org/10.5194/acp-6-3181-2006

Hall, D. K., & Riggs, G. A. (2021a). *MODIS/Terra snow cover daily L3 global 0.05 Deg CMG, version 61*. NASA National Snow and Ice Data Center Distributed Active Archive Center. https://doi.org/10.5067/MODIS/MOD10C1.061

Hall, D. K., & Riggs, G. A. (2021b). *MODIS/Terra snow cover monthly L3 global 0.05 Deg CMG, version 61*. NASA National Snow and Ice Data Center Distributed Active Archive Center. https://doi.org/10.5067/MODIS/MOD10CM.061

Hamilton, D. S., Perron, M. M. G., Bond, T. C., Bowie, A. R., Buchholz, R. R., Guieu, C., et al. (2022). Earth, wind, fire, and pollution: Aerosol nutrient sources and impacts on ocean biogeochemistry. *Annual Review of Marine Science*, *14*(1), 303–330. https://doi.org/10.1146/annurev-marine-031921-013612

Han, J., Dai, H., & Gu, Z. (2021). Sandstorms and desertification in Mongolia, an example of future climate events: A review. *Environmental Chemistry Letters*, *19*(6), 4063–4073. https://doi.org/10.1007/s10311-021-01285-w

Han, L., Tsunekawa, A., & Tsubo, M. (2011). Effect of frozen ground on dust outbreaks in spring on the Eastern Mongolian Plateau. *Geomorphology*, *129*(3), 412–416. https://doi.org/10.1016/j.geomorph.2011.03.005

Jiang, C., Liu, J., Zhang, H., Zhang, Z., & Wang, D. (2019). China's progress towards sustainable land degradation control: Insights from the Northwest arid regions. *Ecological Engineering*, *127*, 75–87. https://doi.org/10.1016/j.ecoleng.2018.11.014

Jin, J., Pang, M., Segers, A., Han, W., Fang, L., Li, B., et al. (2022). Inverse modeling of the 2021 spring super dust storms in East Asia. *Atmospheric Chemistry and Physics*, *22*(10), 6393–6410. https://doi.org/10.5194/acp-22-6393-2022

Jugder, D., Gantsetseg, B., Davaanyam, E., & Shinoda, M. (2018). Developing a soil erodibility map across Mongolia. *Natural Hazards*, *92*(1), 71–94. https://doi.org/10.1007/s11069-018-3409-6

Jugder, D., Shinoda, M., Kimura, R., Batbold, A., & Amarjargal, D. (2014). Quantitative analysis on windblown dust concentrations of PM_{10} ($PM_{2.5}$) during dust events in Mongolia. *Aeolian Research*, *14*, 3–13. https://doi.org/10.1016/j.aeolia.2014.04.005

Kelso, N. V., & Patterson, T. (2010). Introducing natural earth data-Naturalearthdata. com. *Geographia Technica*, *5*(82–89), 25.

Kim, D., Chin, M., Bian, H., Tan, Q., Brown, M. E., Zheng, T., et al. (2013). The effect of the dynamic surface bareness on dust source function, emission, and distribution. *Journal of Geophysical Research: Atmospheres*, *118*(2), 871–886. https://doi.org/10.1029/2012JD017907

Kim, D., Chin, M., Kemp, E. M., Tao, Z., Peters-Lidard, C. D., & Ginoux, P. (2017a). Development of high-resolution dynamic dust source function—a case study with a strong dust storm in a regional model. *Atmospheric Environment*, *159*, 11–25. https://doi.org/10.1016/j.atmosenv.2017.03.045

Kim, D., Chin, M., Remer, L. A., Diehl, T., Bian, H., Yu, H., et al. (2017b). Role of surface wind and vegetation cover in multi-decadal variations of dust emission in the Sahara and Sahel. *Atmospheric Environment*, *148*, 282–296. https://doi.org/10.1016/j.atmosenv.2016.10.051

Kimura, R. (2018). Satellite-based mapping of dust erodibility in northeast Asia. *Natural Hazards*, *92*(1), 19–25. https://doi.org/10.1007/s11069-016-2393-y

Kimura, R., Bai, L., & Wang, J. (2009). Relationships among dust outbreaks, vegetation cover, and surface soil water content on the Loess Plateau of China, 1999–2000. *Catena*, *77*(3), 292–296. https://doi.org/10.1016/j.catena.2009.02.016

Kok, J., Storelvmo, T., Karydis, V., Adebiyi, A., Mahowald, N., Evan, A., et al. (2023). Mineral dust aerosol impacts on global climate and climate change. *Nature Reviews Earth & Environment*, *4*(2), 71–86. https://doi.org/10.1038/s43017-022-00379-5

Kurosaki, Y., & Mikami, M. (2004). Effect of snow cover on threshold wind velocity of dust outbreak. *Geophysical Research Letters*, *31*(3). https://doi.org/10.1029/2003GL018632

Lee, E.-H., & Sohn, B.-J. (2009). Examining the impact of wind and surface vegetation on the Asian dust occurrence over three classified source regions. *Journal of Geophysical Research*, *114*(D6). https://doi.org/10.1029/2008JD010687

Lee, E.-H., & Sohn, B.-J. (2011). Recent increasing trend in dust frequency over Mongolia and Inner Mongolia regions and its association with climate and surface condition change. *Atmospheric Environment*, *45*(27), 4611–4616. https://doi.org/10.1016/j.atmosenv.2011.05.065

Lee, J.-H., & Lee, S.-H. (2022). Modeling a severe wintertime Asian dust event observed in the East Asia region: Sensitivity of the WRF-Chem dust emission schemes. *Atmospheric Pollution Research*, *13*(12), 101599. https://doi.org/10.1016/j.apr.2022.101599

Lee, J.-J., & Kim, C.-H. (2012). Roles of surface wind, NDVI and snow cover in the recent changes in Asian dust storm occurrence frequency. *Atmospheric Environment*, *59*, 366–375. https://doi.org/10.1016/j.atmosenv.2012.05.022

LeGrand, S. L., Polashenski, C., Letcher, T. W., Creighton, G. A., Peckham, S. E., & Cetola, J. D. (2019). The AFWA dust emission scheme for the GOCART aerosol model in WRF-Chem v3.8.1. *Geoscientific Model Development*, *12*(1), 131–166. https://doi.org/10.5194/gmd-12-131-2019

Li, H., Wang, C., Wang, M., Liu, Z., Mamtimin, A., & Pan, X. (2023). A new dataset of erodibility in dust source for WRF-Chem model based on remote sensing and soil texture—application and Validation. *Atmospheric Environment*, *315*, 120156. https://doi.org/10.1016/j.atmosenv.2023.120156

Li, J., Hao, X., Liao, H., Yue, X., Li, H., Long, X., & Li, N. (2022). Predominant type of dust storms that influences air quality over Northern China and future projections. *Earth's Future*, *10*(6), e2022EF002649. https://doi.org/10.1029/2022EF002649

Li, M., Zhang, Q., Kurokawa, J., Woo, J.-H., He, K., Lu, Z., et al. (2017). Mix: A mosaic Asian anthropogenic emission inventory under the international collaboration framework of the MICS-Asia and HTAP. *Atmospheric Chemistry and Physics*, *17*(2), 935–963. https://doi.org/10.5194/acp-17-935-2017

Liu, L., Huang, X., Ding, A., & Fu, C. (2016). Dust-induced radiative feedbacks in North China: A dust storm episode modeling study using WRF-Chem. *Atmospheric Environment*, *129*, 43–54. https://doi.org/10.1016/j.atmosenv.2016.01.019

Liu, Y., Xu, R., D. Ziegler, A., & Zeng, Z. (2022). Stronger winds increase the sand-dust storm risk in Northern China. *Environmental Sciences: Atmosphere*, *2*(6), 1259–1262. https://doi.org/10.1039/D2EA00058J

Mahowald, N., Luo, C., del Corral, J., & Zender, C. S. (2003). Interannual variability in atmospheric mineral aerosols from a 22-year model simulation and observational data. *Journal of Geophysical Research*, *108*(D12). https://doi.org/10.1029/2002JD002821

Mahowald, N. M., Kloster, S., Engelstaedter, S., Moore, J. K., Mukhopadhyay, S., McConnell, J. R., et al. (2010). Observed 20th century desert dust variability: Impact on climate and biogeochemistry. *Atmospheric Chemistry and Physics*, *10*(22), 10875–10893. https://doi.org/10.5194/acp-10-10875-2010

Mao, R., Ho, C.-H., Feng, S., Gong, D.-Y., & Shao, Y. (2013). The influence of vegetation variation on Northeast Asian dust activity. *Asia-Pacific Journal of Atmospheric Sciences*, *49*(1), 87–94. https://doi.org/10.1007/s13143-013-0010-5

Middleton, N. J. (2017). Desert dust hazards: A global review. *Aeolian Research*, *24*, 53–63. https://doi.org/10.1016/j.aeolia.2016.12.001

Mokhtari, M., Gomes, L., Tulet, P., & Rezoug, T. (2012). Importance of the surface size distribution of erodible material: An improvement on the Dust Entrainment and Deposition (DEAD) model. *Geoscientific Model Development*, *5*(3), 581–598. https://doi.org/10.5194/gmd-5-581-2012

Okin, G. S. (2005). Dependence of wind erosion and dust emission on surface heterogeneity: Stochastic modeling. *Journal of Geophysical Research*, *110*(D11). https://doi.org/10.1029/2004JD005288

Okin, G. S. (2008). A new model of wind erosion in the presence of vegetation. *Journal of Geophysical Research*, *113*(F2). https://doi.org/10.1029/2007JF000758

Parajuli, S. P., Stenchikov, G. L., Ukhov, A., Mostamandi, S., Kucera, P. A., Axisa, D., et al. (2022). Effect of dust on rainfall over the Red Sea coast based on WRF-Chem model simulations. *Atmospheric Chemistry and Physics*, *22*(13), 8659–8682. https://doi.org/10.5194/acp-22-8659-2022

Parajuli, S. P., & Zender, C. S. (2017). Connecting geomorphology to dust emission through high-resolution mapping of global land cover and sediment supply. *Aeolian Research*, *27*, 47–65. https://doi.org/10.1016/j.aeolia.2017.06.002

Platnick, S., King, M., & Hubanks, P. (2015). MODIS atmosphere L3 daily product, NASA MODIS adaptive processing system [Dataset]. *Goddard Space Flight Center*. https://modis.gsfc.nasa.gov/data/dataprod/mod08.php

Prospero, J. M., Ginoux, P., Torres, O., Nicholson, S. E., & Gill, T. E. (2002). Environmental characterization of global sources of atmospheric soil dust identified with the Nimbus 7 Total Ozone Mapping Spectrometer (TOMS) absorbing aerosol product. *Reviews of Geophysics*, *40*(1), 2-1-2–31. https://doi.org/10.1029/2000RG000095

Sekiyama, T. T., Tanaka, T. Y., Maki, T., & Mikami, M. (2011). The effects of snow cover and soil moisture on Asian dust: II. Emission estimation by Lidar data assimilation. *SOLA*, *7A*(Special_Edition), 40–43. https://doi.org/10.2151/sola.7A-011

Shao, Y. (2008). *Physics and modelling of wind erosion*. Springer.

Shao, Y., Klose, M., & Wyrwoll, K.-H. (2013). Recent global dust trend and connections to climate forcing. *Journal of Geophysical Research: Atmospheres*, *118*(19), 11107–11118. https://doi.org/10.1002/jgrd.50836

Shepherd, G., Terradellas, E., Baklanov, A., Kang, U., Sprigg, W., Nickovic, S., et al. (2016). Global assessment of sand and dust storms. United Nations Environment Programme. Retrieved from https://api.semanticscholar.org/CorpusID:133358219

Smith, A., Lott, N., & Vose, R. (2011). The integrated surface database: Recent developments and partnerships. *Bulletin of the American Meteorological Society*, *92*(6), 704–708. https://doi.org/10.1175/2011bams3015.1

Smith, W. H., & Sandwell, D. T. (1997). Global sea floor topography from satellite altimetry and ship depth soundings. *Science*, *277*(5334), 1956–1962. https://doi.org/10.1126/science.277.5334.1956

Solomos, S., Abuelgasim, A., Spyrou, C., Binietoglou, I., & Nickovic, S. (2019). Development of a dynamic dust source map for NMME-DREAM v1.0 model based on MODIS Normalized Difference Vegetation Index (NDVI) over the Arabian Peninsula. *Geoscientific Model Development*, *12*(3), 979–988. https://doi.org/10.5194/gmd-12-979-2019

Song, H., Wang, K., Zhang, Y., Hong, C., & Zhou, S. (2017). Simulation and evaluation of dust emissions with WRF-Chem (v3.7.1) and its relationship to the changing climate over East Asia from 1980 to 2015. *Atmospheric Environment*, *167*, 511–522. https://doi.org/10.1016/j.atmosenv.2017.08.051

Tai, A. P. K., Ma, P. H. L., Chan, Y.-C., Chow, M.-K., Ridley, D. A., & Kok, J. F. (2021). Impacts of climate and land cover variability and trends on springtime east Asian dust emission over 1982–2010: A modeling study. *Atmospheric Environment*, *254*, 118348. https://doi.org/10.1016/j.atmosenv.2021.118348

Tan, S.-C., & Wang, H. (2014). The transport and deposition of dust and its impact on phytoplankton growth in the Yellow Sea. *Atmospheric Environment*, *99*, 491–499. https://doi.org/10.1016/j.atmosenv.2014.10.016

Tanaka, T. Y., Sekiyama, T. T., Maki, T., & Mikami, M. (2011). The effects of snow cover and soil moisture on Asian dust: I. A numerical sensitivity study. *SOLA*, *7A*(Special_Edition), 36–39. https://doi.org/10.2151/sola.7A-010

Tang, M., Huang, X., Lu, K., Ge, M., Li, Y., Cheng, P., et al. (2017). Heterogeneous reactions of mineral dust aerosol: Implications for tropospheric oxidation capacity. *Atmospheric Chemistry and Physics*, *17*(19), 11727–11777. https://doi.org/10.5194/acp-17-11727-2017

Tao, M., Chen, L., Wang, Z., Wang, J., Che, H., Xu, X., et al. (2017). Evaluation of MODIS Deep blue Aerosol algorithm in Desert region of East Asia: Ground validation and intercomparison. *Journal of Geophysical Research: Atmospheres*, *122*(19), 10357–10368. https://doi.org/10.1002/2017JD026976

Tao, Y., An, X., Sun, Z., Hou, Q., & Wang, Y. (2012). Association between dust weather and number of admissions for patients with respiratory diseases in spring in Lanzhou. *Science of the Total Environment*, *423*, 8–11. https://doi.org/10.1016/j.scitotenv.2012.01.064

Tegen, I., Harrison, S. P., Kohfeld, K., Prentice, I. C., Coe, M., & Heimann, M. (2002). Impact of vegetation and preferential source areas on global dust aerosol: Results from a model study. *Journal of Geophysical Research*, *107*(D21), 14–27. https://doi.org/10.1029/2001JD000963

Tegen, I., Lacis, A., & Fung, I. (1996). The influence on climate forcing of mineral aerosols from disturbed soils. *Nature*, *380*(6573), 419–422. https://doi.org/10.1038/380419a0

Tegen, I., & Miller, R. (1998). A general circulation model study on the interannual variability of soil dust aerosol. *Journal of Geophysical Research*, *103*(D20), 25975–25995. https://doi.org/10.1029/98JD02345

Tobias, A., Karanasiou, A., Amato, F., Roqué, M., & Querol, X. (2019). Health effects of desert dust and sand storms: A systematic review and meta-analysis protocol. *BMJ Open*, *9*(7), e029876. https://doi.org/10.1136/bmjopen-2019-029876

Ukhov, A., Ahmadov, R., Grell, G., & Stenchikov, G. (2021). Improving dust simulations in WRF-Chem v4.1.3 coupled with the GOCART aerosol module. *Geoscientific Model Development*, *14*(1), 473–493. https://doi.org/10.5194/gmd-14-473-2021

Wang, F., Wang, M., Kong, Y., Zhang, H., Ru, X., & Song, H. (2022). Spatial and temporal variations in spring dust concentrations from 2000 to 2020 in China: Simulations with WRF-chem. *Remote Sensing*, *14*(23), 6090. https://doi.org/10.3390/rs14236090

Wang, L., Shi, Z. H., Wu, G. L., & Fang, N. F. (2014). Freeze/thaw and soil moisture effects on wind erosion. *Geomorphology*, *207*, 141–148. https://doi.org/10.1016/j.geomorph.2013.10.032

Wang, S., Yu, Y., Zhang, X.-X., Lu, H., Zhang, X.-Y., & Xu, Z. (2021). Weakened dust activity over China and Mongolia from 2001 to 2020 associated with climate change and land-use management. *Environmental Research Letters*, *16*(12), 124056. https://doi.org/10.1088/1748-9326/ac3b79

Wang, X., Xia, D., Wang, T., Xue, X., & Li, J. (2008). Dust sources in arid and semiarid China and southern Mongolia: Impacts of geomorphological setting and surface materials. *Geomorphology*, *97*(3), 583–600. https://doi.org/10.1016/j.geomorph.2007.09.006

Wang, Z., Huang, X., Wang, N., Xu, J., & Ding, A. (2020). Aerosol-radiation interactions of dust storm deteriorate particle and ozone pollution in East China. *Journal of Geophysical Research: Atmospheres*, *125*(24). https://doi.org/10.1029/2020JD033601

Wu, C., Lin, Z., Shao, Y., Liu, X., & Li, Y. (2022). Drivers of recent decline in dust activity over East Asia. *Nature Communications*, *13*(1), 7105. https://doi.org/10.1038/s41467-022-34823-3

Wu, J., Kurosaki, Y., Shinoda, M., & Kai, K. (2016). Regional characteristics of recent dust occurrence and its controlling factors in East Asia. *SOLA*, *12*(0), 187–191. https://doi.org/10.2151/sola.2016-038

Xi, X. (2021). Revisiting the recent dust trends and climate drivers using horizontal visibility and present weather observations. *Journal of Geophysical Research: Atmospheres*, *126*(9), e2021JD034687. https://doi.org/10.1029/2021JD034687

Yang, L., Zhang, S., Huang, Z., Yang, Y., Wang, L., Han, W., & Li, X. (2021a). Characteristics of dust events in China from 2015 to 2020. *Atmosphere*, *12*(8), 952. https://doi.org/10.3390/atmos12080952

Yang, S., Wang, Z., Huang, X., Wang, W., Sheng, L., & Zhou, Y. (2021b). Meteorological feedback and eco-environmental impact of Asian dust: A simulation study. *Atmospheric Environment*, *253*, 118350. https://doi.org/10.1016/j.atmosenv.2021.118350

Yang, Y., Wang, Z., Lou, S., Xue, L., Lu, J., Wang, H., et al. (2022). Strong ozone intrusions associated with super dust storms in East Asia. *Atmospheric Environment*, *290*, 119355. https://doi.org/10.1016/j.atmosenv.2022.119355

Yin, Z., Huo, Q., Ma, X., Zhang, Y., Ma, X., & Wang, H. (2023). Mechanisms of dust source accumulation and synoptic disturbance triggering the 2023 spring sandstorm in northern China. *Trans Atmos Sci*, *46*(3), 321–331.

Yin, Z., Wan, Y., Zhang, Y., & Wang, H. (2022). Why super sandstorm 2021 in North China? *National Science Review*, *9*(3), nwab165. https://doi.org/10.1093/nsr/nwab165

Zender, C. S., Bian, H., & Newman, D. (2003). Mineral Dust Entrainment and Deposition (DEAD) model: Description and 1990s dust climatology. *Journal of Geophysical Research*, *108*(D14). https://doi.org/10.1029/2002JD002775

Zender, C. S., & Kwon, E. Y. (2005). Regional contrasts in dust emission responses to climate. *Journal of Geophysical Research*, *110*(D13). https://doi.org/10.1029/2004JD005501

Zeng, Y., Wang, M., Zhao, C., Chen, S., Liu, Z., Huang, X., & Gao, Y. (2019). WRF-chem v3.9 simulations of the east Asian dust storm in May 2017: Modeling sensitivities to dust emission and dry deposition schemes (preprint). *Atmospheric Sciences*. https://doi.org/10.5194/gmd-2019-310

Zhang, Z., Liang, J., Ji, H., Li, M., Ding, J., Tang, C., et al. (2024). Quantifying mineral dust emissions on the Tibetan plateau with a modified dust source map. *Geophysical Research Letters*, *51*(1), e2023GL107042. https://doi.org/10.1029/2023GL107042

Zhou, D., Ding, K., Huang, X., Liu, L., Liu, Q., Xu, Z., et al. (2018). Transport, mixing and feedback of dust, biomass burning and anthropogenic pollutants in eastern Asia: A case study. *Atmospheric Chemistry and Physics*, *18*(22), 16345–16361. https://doi.org/10.5194/acp-18-16345-2018

Zou, X. K., & Zhai, P. M. (2004). Relationship between vegetation coverage and spring dust storms over northern China. *Journal of Geophysical Research*, *109*(D3). https://doi.org/10.1029/2003JD003913